Title

Organ-specific fuel rewiring in acute and chronic hypoxia redistributes glucose and fatty acid metabolism

Journal

Cell Metabolism, 35(3)

ISSN

1550-4131

Authors

Midha, Ayush D

Zhou, Yuyin

Queliconi, Bruno B

et al.

Publication Date

2023-03-01

DOI

10.1016/j.cmet.2023.02.007

Peer reviewed

HHS Public Access

Author manuscript

Cell Metab. Author manuscript; available in PMC 2024 March 07.

Published in final edited form as:

Cell Metab. 2023 March 07; 35(3): 504–516.e5. doi:10.1016/j.cmet.2023.02.007.

Organ-Specific Fuel Rewiring in Acute and Chronic Hypoxia Redistributes Glucose and Fatty Acid Metabolism

Ayush D. Midha[1,2,3,4,7], **Yuyin Zhou**[1,2,7], **Bruno B. Queliconi**[1,2], **Alec M. Barrios**[1,2], **Augustinus G. Haribowo**[1,2], **Brandon T. L. Chew**[1,2,5], **Cyril O. Y. Fong**[6], **Joseph E. Blecha**[6], **Henry VanBrocklin**[6], **Youngho Seo**[6], **Isha H. Jain**[1,2,8,*]

[1]Gladstone Institutes, San Francisco, CA, 94158, USA

[2]Department of Biochemistry and Biophysics, University of California, San Francisco, CA 94158, USA

[3]Medical Scientist Training Program, University of California, San Francisco, CA 94143, USA

[4]Tetrad Graduate Program, University of California, San Francisco, San Francisco, CA 94158, USA

[5]Pharmaceutical Sciences and Pharmacogenomics Graduate Program, University of California, San Francisco, San Francisco, CA 94158, USA

[6]Department of Radiology and Biomedical Imaging, University of California, San Francisco, CA 94107, USA

[7]These authors contributed equally

[8]Lead Contact

SUMMARY:

Oxygen deprivation can be detrimental. However, chronic hypoxia is also associated with decreased incidence of metabolic syndrome and cardiovascular disease in high-altitude populations. Previously, hypoxic fuel rewiring has primarily been studied in immortalized cells. Here, we describe how systemic hypoxia rewires fuel metabolism to optimize whole-body adaptation. Acclimatization to hypoxia coincided with dramatically lower blood glucose and adiposity. Using *in vivo* fuel uptake and flux measurements, we found that organs partitioned fuels differently during hypoxia adaption. Acutely, most organs increased glucose uptake and suppressed aerobic glucose oxidation, consistent with previous *in vitro* investigations. In contrast, brown adipose tissue and skeletal muscle became “glucose savers,” suppressing glucose uptake

*Correspondence: Isha.Jain@gladstone.ucsf.edu.

AUTHOR CONTRIBUTIONS

IHJ, ADM, YZ, BBQ, AMB conceived the project and performed the experiments. IHJ, ADM, YZ designed the experiments and analyzed the data. ADM, IHJ wrote the manuscript. COYF, JEB prepared PET radiotracers. BTLC and AGH assisted with tissue PO_2 measurements. HV, YS designed PET radiotracers and assisted with data analysis.

DECLARATION OF INTERESTS

IHJ is a consultant for Maze Therapeutics and has a patent related to hypoxia therapy for mitochondrial disorders.

by 3–5-fold. Interestingly, chronic hypoxia produced distinct patterns: the heart relied increasingly on glucose oxidation, and unexpectedly, the brain, kidney, and liver increased fatty acid uptake and oxidation. Hypoxia-induced metabolic plasticity carries therapeutic implications for chronic metabolic diseases and acute hypoxic injuries.

eTOC

Midha et al. show that functional adaptation to hypoxia is accompanied by organ-specific metabolic rewiring. Acute hypoxia promotes glucose uptake in most organs while reducing oxygen-consuming glucose oxidation. Chronic hypoxia promotes fatty acid metabolism in the brain, liver, and kidney while increasing glucose oxidation in the heart.

Graphical Abstract

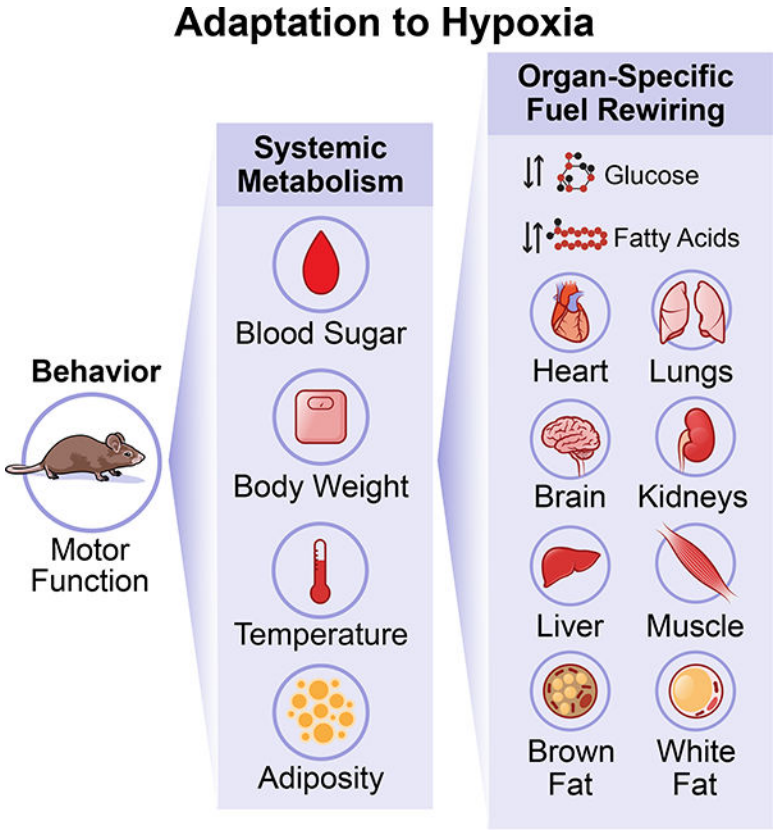

Keywords

Hypoxia; fuel rewiring; organ-specific metabolism; fuel uptake; glucose metabolism; fatty acid metabolism; TCA cycle; PET scan; isotope tracing

INTRODUCTION

Oxygen deprivation contributes to several leading causes of mortality in developed nations —myocardial infarction (MI), stroke, and respiratory failure. While oxygen deprivation

can have devastating health consequences, chronic hypoxia can also stimulate protective adaptations. For example, a gradual ascent to altitude reduces the incidence of altitude sickness, high-altitude pulmonary edema (HAPE), and high-altitude cerebral edema (HACE).[1] At the organ level, exposure to transient, sublethal ischemia increases resilience to future ischemic events, known as ischemic preconditioning.[2–6] Moreover, ischemic injury to non-cardiac tissue confers resilience to MI, known as remote ischemic preconditioning.[7,8] Thus, gradual adaptation to hypoxia can impart significant health advantages. This adaptation is partially mediated by the activation of hypoxia-inducible transcription factors (HIF),[9–11] which promote erythropoiesis and angiogenesis to enable survival at lower oxygen levels.[12,13] While previous work has focused extensively on these transcriptional programs, metabolic adaptations to hypoxia remain incompletely understood at the whole-body level.

The metabolic responses to hypoxia are especially important given the striking observation that high-altitude residents are paradoxically protected against a range of metabolic conditions. More than 2 million individuals reside at an altitude greater than 4500m at an oxygen level that translates to an 11% fraction of inspired oxygen (F_iO_2) (compared to 21% at sea level).[14] Over a dozen studies have found that high-altitude residents have significantly lower rates of hyperglycemia, hypercholesterolemia, and obesity[15–23] and reduced mortality from coronary artery disease and stroke.[24–26] Oxygen deprivation alone can also have therapeutic benefits, independent of altitude. For example, low blood hemoglobin levels are associated with improved glucose homeostasis, decreased insulin resistance, and lower LDL and triglyceride levels in mice and humans.[27] Additionally, we recently showed that hypoxia exposure extends lifespan, reverses neurological lesions, and treats functional deficits in a mouse model of monogenic mitochondrial disease.[28] These observations suggest that shifts in oxygen availability prompt a rewiring of organ-level and systemic metabolism that may be therapeutic.

Technological advances have enabled comprehensive, unbiased investigation of systemic metabolism, revealing the considerable metabolic flexibility and fuel rewiring of mammals in response to physiological stimuli. For example, endurance exercise in humans rapidly activates skeletal muscle glucose uptake and fatty acid oxidation.[29] Conversely, fasting activates a transition away from glucose utilization, mobilizing lipids, ketone bodies, and amino acids.[30] These metabolic switches optimize resource consumption to meet shifting energetic needs.

The findings of significant metabolic flexibility and sustained adaptation to hypoxia raise an important question—how do mammalian organs reorganize their fuel preferences and metabolic pathways to meet energy demands in oxygen-limited environments? The canonical view of hypoxia metabolism emphasizes a switch from oxidative phosphorylation to increased anaerobic glycolysis, suggesting a shift away from fatty acid metabolism towards glucose utilization. However, this perspective stems primarily from studies in cancer cell lines.[31–33] Uniform whole-body reliance on anaerobic glycolysis is unlikely to be adaptive as it would result in rapid glucose depletion and severe lactic acidosis. Thus, it is more likely that different organs rewire their metabolism based on local oxygenation, organ-specific functions, and nutrient availability.

To test this hypothesis, we measured fuel uptake and metabolic flux in live mice exposed to acute and chronic ambient hypoxia using positron emission tomography and isotope-labeled fuel tracers. As expected, acute hypoxia increased glucose uptake in most organs while reducing the mitochondrial oxidation of glucose. Notable exceptions included skeletal muscle and brown fat, which serve as "glucose-saving" organs by decreasing glucose uptake in acute hypoxia. In chronic hypoxia, organs transformed their metabolism in unique ways. The heart increased its dependence on mitochondrial glucose oxidation, while the brain, kidney, and liver promoted fatty acid uptake to feed the TCA cycle. These organ-specific changes coincided with reduced body fat, dramatically reduced blood glucose levels, and improvements in hypoxia-induced perturbations in locomotor function. This comprehensive characterization elucidates how organs contribute differently to systemic hypoxia adaptation while producing a catabolic state. These findings highlight some mechanisms underlying hypoxia-induced improvements in metabolic fitness and organ resilience to oxygen deprivation.

RESULTS

Impaired locomotor function in acute hypoxia is rescued over time

To establish a model of hypoxia adaptation, we began by assessing spontaneous movement and fitness, since these traits are known to be acutely impaired in humans at high altitude. We housed young adult mice in three different oxygen tensions (21%, 11%, and 8% F_iO_2) for four different time periods (3 hours, 24 hours, 1 week, and 3 weeks) representing acute, subacute, and chronic hypoxia. 21% represents the oxygen tension of room air at sea level, and 11% and 8% correspond to altitudes of 4500m and greater than 5000m, respectively. These two F_iO_2s were chosen because they represent significant hypoxia that is survivable in mice and humans. Of note, 2 million people live above 4500m and 300,000 people live above 5000m.[14]

To evaluate spontaneous movement, we conducted an open field assay, measuring distance travelled, speed, and resting time in a controlled atmosphere. Acutely, oxygen deprivation significantly reduced spontaneous movement and increased resting time, but by 3 weeks, mice exposed to hypoxia increased their movement to near normal levels (Fig 1A–D). We also conducted pole tests as an integrated assessment of motor function, including coordination, strength, and speed.[34] Mice were placed at the top of a pole facing up or down, and we measured the latency to descend. In both starting positions, mice exposed to 8% F_iO_2 for 24 hours took significantly longer to descend than mice exposed to 21% F_iO_2. By 3 weeks of exposure, however, the latency to descend among the hypoxia groups was comparable to the normoxic controls (Fig 1E–F). Together, these results indicate that acute hypoxia reduces spontaneous motion and motor coordination, but adaptation over several weeks rescues these motor deficits.

Physiological responses to hypoxia include systemic metabolic rewiring

To identify the mechanisms by which acute locomotor defects improve under chronic hypoxia, we carefully monitored physiological markers known to respond to hypoxia, including hemoglobin, blood CO_2, and body temperature. As expected, hemoglobin levels

doubled after 3 weeks in 8% F_iO_2 (Fig 2A), matching previous human studies.[35,36] Another well-known response to acute hypoxia is hyperventilation, which increases the expiration of CO_2. As a result, acute hypoxia lowered total blood CO_2, but over 3 weeks, this parameter returned to normal (Fig 2B).

In acute hypoxia, we also observed a dramatic drop in body temperature (anapyrexia), but this normalized over the following weeks (Fig 2C). Hypoxia-induced anapyrexia has previously been observed in other mammals, including rats,[37] golden hamsters,[38] naked mole rats,[39] and humans.[40] The mechanism underlying this phenomenon remains unknown, but adaptive benefits in acute hypoxia may include preserved energy stores, increased hemoglobin-O_2 binding affinity, and a dampened hyperventilation response to hypoxia.[41] Indeed, lowering body temperature confers neuroprotection in hypoxic-ischemic encephalopathy.[42] However, the reversal of hypoxia-induced anapyrexia over time indicates that persistently low body temperature is not required for survival in chronic hypoxia.

Given that thermogenesis requires significant energy expenditure, we asked whether mice exhibited changes in body weight and energy intake during their adaptation to hypoxia. Acute oxygen deprivation stimulated a significant decline in body weight that was partially reversed over time. Four days in 8% F_iO_2 lowered body weights by 20%, but by three weeks, weights had partially recovered and stabilized at 10% below baseline (Fig 2D). The acute drop in body weight tracked closely with a similar reduction in food consumption (Fig 2E). Previous studies have demonstrated that paired feeding rescues hypoxia-induced weight loss,[43] so depressed food intake is the likely cause of the observed weight loss. Research in humans has similarly demonstrated a rapid decline in food consumption at even more moderate hypoxia conditions.[44] We found that after one week of hypoxia, food consumption returned to normal, matching the time course of body temperature recovery.

The precise signaling cascade driving hypoxia-induced anorexia remains unknown. Increased leptin secretion, which promotes satiety, has been proposed as a possible mechanism, but human studies have produced conflicting results,[44–46] perhaps linked to confounding variables such as ambient temperature, barometric pressure, and sleep at altitude. By contrast, our experimental setup allowed us to assess the effects of oxygen deprivation alone. We collected blood between 10am and 12pm without fasting mice to avoid influencing the results with exogenous interventions. From these hormone measurements, we found that leptin levels were elevated in mice housed at 8% F_iO_2 for 24 hours (Fig 2F), which corresponds to the timepoint with the largest drop in food intake. In addition, levels of ghrelin, which promotes food intake, were significantly lower at 3 hours but returned to normal at 24 hours and were significantly elevated at 1 week (Fig 2F). These data suggest that hormonal responses to hypoxia may contribute to acute anorexia.

Regardless of its cause, the sustained weight loss in hypoxia led us to hypothesize that oxygen-deprived mice may activate starvation-response pathways. Consistent with this hypothesis, hypoxia produced a significant increase in blood urea nitrogen (BUN) that was time- and oxygen dose-responsive (Fig 2G). Blood urea is produced from ammonia generated by protein degradation, and this urea is excreted by the kidney. Therefore, elevated BUN can indicate kidney injury or elevated rates of protein catabolism.[47] However, we

observed that serum creatinine levels, another marker of kidney injury, remained below the detectable threshold throughout hypoxia treatment. Therefore, our observation of elevated BUN indicates a perturbed nitrogen balance most likely caused by protein catabolism. Consistent with these findings, altitude studies have found that chronic hypoxia reduces skeletal muscle mass,[48,49] and oxygen deprivation in cell lines activates protein catabolism to meet energy demands.[50]

Based on the time-dependent metabolic changes in hypoxia, we sought to determine the precise tissue oxygen tensions in acute and chronic exposure to 8% F_iO_2. To measure tissue oxygenation, we intubated mice and ventilated them at the appropriate F_iO_2. Subsequently, a Clark-type microsensor was inserted into different organs to measure the partial pressure of oxygen. As expected, acute hypoxia induced a precipitous drop in oxygen levels across organs. In chronic hypoxia, however, some organs, including the heart, brain, and liver, exhibited a partial recovery in oxygenation (Fig 2H). Different organs had different baseline oxygen tensions and patterns of recovery, highlighting the organ-specific changes on the backdrop of ambient hypoxia. Together, these findings demonstrate that adaptation to hypoxia involves systemic metabolic rewiring, even as some organs partially recover their oxygenation.

Chronic hypoxia lowers blood glucose levels and alters organ-level glucose uptake

Given the dramatic metabolic changes in hypoxia and the prior evidence of reduced diabetes incidence among high-altitude populations, we asked whether hypoxia alone could alter systemic glucose homeostasis. Exposure to 8% F_iO_2 induced a significant time- and dose-dependent reduction in fasted and fed glucose levels (Fig 3A). As expected, normoxic mice had fasted glucose levels around 100 mg/dL and fed glucose levels around 150 mg/dL. At 3 hours of treatment, fasted and fed glucose levels were slightly lower before recovering to normal at 24 hours. By 1 week, though, both fed and fasted blood glucose levels cratered to ~55 mg/dL. Despite the return to normal food consumption at 3 weeks, fasted and fed blood glucose levels were both less than 40 mg/dL. This dramatic 3–4-fold decrease in circulating glucose was not accompanied by any overt detrimental effects. To the contrary, behavior recovered to normoxic states at chronic timepoints (Fig 1).

To explain this observation, we considered hypoxia-induced changes in pancreatic islet endocrine activity. Insulin levels were elevated at acute timepoints but returned to normal at 1 week and 3 weeks in 8% F_iO_2 (Fig 3B). Conversely, glucagon levels were decreased at 24 hours and highly varied at 1 week before returning to normal (Fig 3B). Neither hormone was significantly perturbed in chronic hypoxia. Therefore, changes in insulin and glucagon production are unlikely to explain the dramatic hypoglycemia in chronic hypoxia.

We also considered that diminished transcription of gluconeogenesis genes may cause hypoxia-induced hypoglycemia. To test this, we measured gene expression of *Pcx* (pyruvate carboxylase), *Pck1* (PEP carboxykinase), and *G6pc* (glucose 6-phosphatase) in the liver and kidney, the two major gluconeogenic organs. Surprisingly, we found that at 24 hours, both organs upregulated *Pcx*, and the kidney exhibited higher expression of *Pck1* (Fig S1A). Interestingly, at this timepoint, both fed and fasted glucose levels also returned to normal levels (Fig 3A). In chronic hypoxia, we observed no changes in the expression of levels of

these 3 genes, so transcriptional suppression of gluconeogenesis genes is unlikely to explain hypoxia-induced hypoglycemia.

We therefore asked whether organs increased glucose consumption as a function of time in hypoxia. We measured organ-specific glucose uptake using PET-CT imaging with an injected 2-deoxy-2-[^{18}F]fluoro-D-glucose (FDG) tracer. FDG is taken up by cells through glucose transporters; after phosphorylation, the molecule is trapped within cells and does not undergo further metabolism.[51] Thus, the radioactive ^{18}F signal can be imaged as a measure of glucose uptake. We conducted FDG PET scans in mice housed at 21% and 8% F_iO_2 for 3 hours, 24 hours, 1 week, and 3 weeks. We also extracted organs and used a gamma counter to quantify the ^{18}F signal from each organ.[52]

In normoxia, the major glucose consumers were the heart and brown adipose tissue (BAT), followed by the lungs and brain (Fig 3C). In response to hypoxia, most organs acutely increased their glucose uptake, but the kinetics differed across organs (Fig 3D–E, S1B). For example, glucose uptake increased after as little as 3 hours in hypoxia for the brain and kidney, compared to 1 week for the heart. In chronic hypoxia, the heart and brain increased glucose uptake and simultaneously upregulated expression of the glucose transporter gene *Slc2a1* (Fig S1C). These organ-specific differences may implicate the time required for organs to adapt to ischemic injury or systemic hypoxic events.

These results are consistent with the classical teachings of hypoxia adaptation in proliferating cells. In this model, hypoxia promotes glucose uptake, upregulates glycolytic enzymes, and increases lactate excretion as the end-product of anaerobic glycolysis.[31] Contrary to this traditional view and the overall trend of increased glucose uptake, two organs substantially decreased their glucose consumption in acute hypoxia: skeletal muscle and BAT. In skeletal muscle, glucose uptake returned to baseline at 3 weeks, a pattern that mirrors the acute impairment and subsequent improvement in locomotor activity. Reduced movement during acute hypoxia likely preserves circulating glucose for other organs because skeletal muscle contraction promotes glucose uptake.[53]

In BAT, glucose uptake was decreased by nearly five-fold persistently across acute and chronic hypoxia. Interestingly, both organs contribute to thermoregulation; skeletal muscle activity enables shivering thermogenesis, and BAT metabolism drives non-shivering thermogenesis.[54] The acute suppression of glucose uptake in both organs coincided with a significant drop in body temperature (Fig 2C). A study in naked mole rats showed that exposure to 7% F_iO_2 rapidly lowered body temperature and reduced UCP1 expression in brown fat, which is required for thermogenesis.[39] Therefore, the improvement in body temperature over time may emerge due to a switch away from BAT thermogenesis as skeletal muscle metabolism recovers.

Chronic hypoxia reduces fat accumulation and alters organ-level uptake of free fatty acids

After observing such dramatic changes in glucose utilization, we asked whether hypoxia affects additional major fuel sources. To this end, we characterized hypoxia-induced changes in systemic and organ-specific fatty acid metabolism. We measured the fat content in mice by conducting dual-energy X-ray absorptiometry (DEXA) scans and weighing epididymal

white adipose tissue (eWAT), a visceral fat depot. Chronic hypoxia reduced total fat mass and the weight of eWAT depots (Fig 4A). Chronic hypoxia also reduced total lean mass, but to a smaller degree than the reduction in fat mass (Fig S2A–C). Strikingly, we observed reduced adiposity despite a recovery in food intake after the first week of hypoxia treatment. Along with the observed reduction in blood glucose levels, these data provide experimental support to the hypothesis that chronic adaptation to hypoxia promotes the catabolism of stored fuels.

To investigate the mechanism underlying reduced fat accumulation in chronic hypoxia, we measured fatty acid uptake in organs. Analogous to the FDG PET scans, we conducted PET scans using 18-[18F]fluoro-4-thia-palmitate (FTP), a metabolically trapped free fatty acid (FFA) tracer.[55] FTP resembles the saturated fatty acid palmitate, the most abundant FFA in circulation. FTP undergoes mitochondrial uptake through the carnitine shuttle before being trapped in the mitochondria.[56]

As expected, FTP PET scans showed that in normoxia, the heart, liver, and kidney were the most significant consumers of circulating palmitate (Fig 4B). On the other hand, the brain exhibited ten-fold lower FFA uptake than the heart. Acute hypoxia had no significant effect on FFA metabolism across organs. Meanwhile, chronic hypoxia prompted a significant increase in FFA uptake in the liver, kidney, brain, muscle, and spleen (Fig 4C–D, S2D). Interestingly, the brain and muscle both exhibited minimal palmitate uptake at baseline, and their increased palmitate uptake in chronic hypoxia coincided with upregulated expression of *Cd36*, which facilitates fatty acid transport[57] (Fig S2E). Increased fatty acid uptake across multiple organs contradicts classical teachings from cancer cell lines of decreased fatty acid metabolism in hypoxia.[58,59]

Hypoxia rewires metabolic flux of major fuel sources into the TCA cycle

Given the importance of oxygen in mitochondrial oxidative metabolism, we next investigated how hypoxia affects the shuttling of circulating fuels into the TCA cycle. We conducted separate bolus injections of the stable isotopes U-^{13}C-glucose and U-^{13}C-palmitate and extracted organs 20 minutes later. The concentrations of these tracers in plasma varied slightly across conditions, reflecting different baseline concentrations of circulating glucose and palmitate in hypoxia (Fig S3A). Next, we traced the conversion of circulating carbons from glucose and palmitate into the TCA intermediates succinate, fumarate, and malate and the TCA-derived amino acid glutamate. The fractional labeling of TCA metabolites, as determined by LC-MS analysis of extracted organs, represents the use of the injected fuels to feed the TCA cycle (Fig 5A, S3B–C). Because the tracer measurements were not conducted at steady state, the exact fractional contributions of glucose and palmitate to downstream metabolites cannot be determined, and enrichments of the isotope label cannot be precisely compared across different organs. Nevertheless, increased enrichment of the isotope label in TCA metabolites implies increased production of TCA intermediates from the labeled fuel relative to other sources.

As expected, we found that in every organ, acute hypoxia reduced the production of TCA metabolites from circulating glucose (Fig 5B–C, S4A). This finding was most pronounced in the heart and skeletal muscle (Fig 5B–C). This pattern coincided with increased glucose

uptake in many organs, suggesting the consumption of glucose for anaerobic glycolysis or other, non-TCA fates. This finding is consistent with a hypoxia-induced blockade of pyruvate dehydrogenase (PDH) activity by HIF.[60] Notably, we observed no such blockade of mitochondrial fatty acid oxidation in acute hypoxia. In all organs, relative palmitate-derived production of TCA metabolites remained steady or even elevated in acute hypoxia (Fig 5B, 5D, S4B).

In chronic hypoxia, however, organs exhibited distinct patterns of glucose oxidation into the TCA cycle. In the heart, glucose-derived production of TCA metabolites was significantly increased relative to normoxia. On the other hand, brown fat, the kidney, and the brain exhibited a significant decrease in glucose-derived TCA metabolites relative to normoxia (Fig 5C, S4A).

Meanwhile, chronic hypoxia significantly increased the contribution of circulating palmitate to the TCA cycle in the kidney, brain, and liver (Fig 5D, S4B). Of note, this 2–3-fold increase in fatty acid oxidation into the TCA cycle mirrored the 2–3-fold increase in FTP-uptake observed in these organs during chronic hypoxia. This upregulation of fatty acid uptake and oxidation in chronic hypoxia belies classical teachings of suppressed oxidative metabolism during hypoxia.

Based on these observations, we identify distinct metabolic classes of organs in chronic hypoxia. The heart stands alone as an increased glucose oxidizer, shuttling carbons from circulating glucose into the mitochondria to feed the TCA cycle. On the other hand, the kidney, liver, and brain mobilize circulating palmitate for mitochondrial metabolism. Finally, BAT suppresses the entry of glucose-derived carbons into the TCA cycle. Altogether, these findings highlight the unique metabolic contributions of different organs to systemic hypoxia adaptation.

DISCUSSION

Acute disruptions in oxygen availability can be lethal. Nevertheless, adaptation to hypoxia at high altitude confers significant metabolic benefits, including improved glycemic control,[21] reduced coronary artery disease mortality,[25] and improved exercise capacity.[61] Mammals can adapt to hypoxia through several known mechanisms, including erythropoiesis,[12,13] angiogenesis,[13,62] and shifts in renal bicarbonate handling.[63] However, the study of metabolic adaptations to hypoxia has thus far been largely limited to the study of cancer cell lines. As a result, the canonical view of hypoxia metabolism focuses on a cellular shift from oxidative phosphorylation to anaerobic glycolysis. However, hypoxia metabolism at the organ and whole-body resolutions has not been systematically characterized.

Here, we show that adaptation to hypoxia entails a systemic metabolic transformation, lowering circulating blood glucose. This is consistent with multiple human altitude studies, which have found reduced blood glucose levels and improved glycemic control among those who live above 3000m (approximately 12.5% F_iO_2).[64] In mice, we found that this hypoglycemia was accompanied by slightly lower insulin levels, significant loss of adiposity, and an increase in circulating BUN, a marker of protein degradation. Altogether, these

findings suggest that chronic hypoxia promotes a systemic catabolic phenotype despite the normalization of body weight. This whole-body metabolic phenotype was accompanied by organ-specific shifts in the uptake and mitochondrial oxidation of circulating fuel sources.

Acutely, most organs responded to hypoxia by increasing glucose uptake while limiting the entry of glucose-derived carbons into the TCA cycle. This pattern indicates increased usage of glucose for non-mitochondrial metabolism (including anaerobic glycolysis), which matches the classical view of adaptation to hypoxia. Meanwhile, brown fat and skeletal muscle deviated from this trend by decreasing their glucose uptake in acute hypoxia, serving as “glucose savers” for other organs that may have a greater need for glucose. Notably, the functions of both organs (thermogenesis and locomotion, respectively) were impaired in acute hypoxia. The partitioning of glucose in acute hypoxia implies that the non-vital functions of thermogenesis and locomotion are compromised to prioritize vital functions of other organs.

In chronic hypoxia, metabolic reprogramming varied significantly across organs (Fig 6). The heart consumed significant amounts of glucose and fatty acids in normoxia but in chronic hypoxia, shifted toward glucose uptake to feed the TCA cycle. These findings are consistent with prior evidence that chronic hypoxia increases the heart’s dependence on glucose.[65] Meanwhile, the brain shifted in the opposite direction, relying more heavily on circulating fatty acids to feed the TCA cycle. Despite this shift in mitochondrial metabolism, the brain still increased its glucose uptake significantly, suggesting alternate, non-mitochondrial fates for this glucose. Increased glucose consumption by the heart and brain likely contributed to the persistent hypoglycemia we observed in hypoxic mice. Meanwhile, the liver and kidney, which were both major fatty acid consumers in normoxia, further increased their fatty acid oxidation in hypoxia by 2–3-fold. Finally, in BAT, glucose uptake and oxidation remained suppressed in chronic hypoxia, and skeletal muscle returned both glucose uptake and oxidation to normal levels.

These organ-specific patterns were confirmed by both PET scans and isotope-labeled tracer experiments. Interestingly, the tracer experiments revealed some differences in label enrichment between TCA metabolites, suggest changes in metabolic regulation not only at the level of fuel entry into the TCA cycle but also in steps within the TCA cycle. Indeed, the TCA cycle is not a unidirectional pathway but a dynamic carousel with a mixture of oxidative, reductive, and anaplerotic reactions.[66] We found, for example, that the labeling patterns of fumarate in some tissues differed from those of succinate and malate. This may reflect changes in the metabolism of other pathways that produce fumarate, including the purine nucleotide cycle, tyrosine metabolism, and the urea cycle. Alternatively, this discrepancy may be a consequence of changes in succinate dehydrogenase activity, which can reflect alterations in the CoQ redox state.[67] Future experiments will involve isotope-labeled tracers using alternate sources of fumarate and measurements of organ-level CoQ redox changes in acute and chronic hypoxia.

Altogether, our findings support different rationales for metabolic rewiring in acute versus chronic hypoxia. In acute hypoxia, the primary goal may be to conserve fuel sources for organs with the most vital functions (e.g., heart, brain, liver) at the expense of

more acutely dispensable functions (e.g., locomotion or precise thermoregulation). In this case, suppressing energy demand in such organs preserves both oxygen and fuel supply. However, on the chronic timescales, organisms likely need to reactivate normal physiological functions, requiring efficient ATP production across all organs. This is achieved by selectively partitioning glucose and fatty acids depending on energy demands, metabolic flexibility, and local oxygenation of different organs. These findings also raise related questions about tumor hypoxia—the metabolic features of acutely hypoxic cancer cells may vary from those of tumors that are chronically deprived of oxygen. As in healthy organs, the effects of hypoxia likely vary in different tumors based on the local oxygenation, levels of hypoxia-induced vascularization, and cell-specific metabolic demands.

Considering the increased oxygen demands of fatty acid oxidation, we did not expect to identify organs that significantly promoted fatty acid oxidation in chronic hypoxia.[68] However, different organs have different baseline PO_2 levels and oxygen-consuming needs in normoxia. Therefore, some organs may maintain their fatty acid oxidation in hypoxia, saving glucose for locations that may rely more on glucose uptake. Our data indicate that this phenomenon is maintained by an organ-specific increase in fatty acid oxidation in the liver, kidney, and brain.

The identification of the brain as an increased fatty acid consumer in chronic hypoxia was particularly unexpected. Ordinarily, the brain relies on glucose consumption for energy supply and, when fasted, on ketone bodies.[69] Nevertheless, recent studies have demonstrated a capacity for low rates of fatty acid oxidation in the brain.[70] The brain's increased fatty acid oxidation in chronic hypoxia suggests an improved supply of oxygen over the course of adaptation to hypoxia, as suggested by our tissue PO_2 measurements. Indeed, severe chronic hypoxia has been shown to promote angiogenesis in the brain.[71] Moreover, the hypoglycemia in chronic hypoxia may activate molecular starvation signals, which promote glial fatty acid oxidation and ketogenesis to supply fuel to neurons.[72] In this study, we focused on organ-level metabolic rewiring. Future studies will focus on specific cell types and regional effects within organs.

Collectively, our findings carry relevance for many metabolic conditions. In chronic hypoxia, we observed an increase in the consumption of circulating fuels by most organs. This may drive a starvation-like program that prevents cardiometabolic diseases caused by excess nutrient storage. Indeed, non-alcoholic fatty liver disease, type 2 diabetes, and atherosclerosis are all worsened by weight gain, hyperglycemia, and lipid accumulation. In chronic hypoxia, these risk factors were all reversed, which may contribute to the lower burden of chronic metabolic diseases among high-altitude populations. Furthermore, organ-specific fuel rewiring in adaptation to hypoxia offers a metabolic starting point for maintaining function during acute disruptions in oxygen supply. Altogether, our results highlight the remarkable mammalian capacity for metabolic flexibility during hypoxia, which we could eventually harness for therapeutic ends.

Limitations of Study

All experiments were conducted in C57BL/6J mice housed at room temperature and fed chow diets. In addition, we focused on glucose and free fatty acid metabolism, but other

circulating fuels may exhibit changes in hypoxia. It is possible that dietary manipulations (e.g., high fat diet, ketogenic diet, or amino acid-restricted diets) and changes in other parameters (e.g., temperature, strain) will result in unique whole-body metabolic rewiring in hypoxia. Future work will incorporate these diets, trace additional fuel sources (lactose, ketones, and amino acids), and identify other metabolic fates of circulating nutrients (pentose phosphate pathway, gluconeogenesis, and one-carbon metabolism).

STAR METHODS

RESOURCE AVAILABILITY

Lead Contact—Further requests for resources should be directed to and will be fulfilled by the Lead Contact, Isha H. Jain (Isha.Jain@gladstone.ucsf.edu).

Materials Availability—All reagents generated in this study are available from the Lead Contact with a completed Materials Transfer Agreement.

Data and Code Availability—All data reported in this paper are included as Data S1.

This paper does not report original code.

Any additional information required to reanalyze the data reported in this paper is available from the lead contact upon request.

EXPERIMENTAL MODEL AND SUBJECT DETAILS

Animal model—Male C57BL/6J (#000664) mice (7–11 weeks old) from The Jackson Laboratory were used for all animal experiments. Mice were housed at 24°C on a 12h:12h light:dark cycle and were fed a chow diet (PicoLab 5058). Cages were randomly allocated to normoxic or hypoxic chambers within the Gladstone Institutes animal facility. Hypoxia was simulated in chambers by mixing N_2 (Airgas), O_2 (Airgas, Praxair), and room air using gas regulators. F_iO_2 and CO_2 levels were checked daily and continuously monitored wirelessly. To inhibit the accumulation of CO_2, soda lime (Fisher Scientific) was added to each chamber. Mouse experiments were approved by the Gladstone Institutes Institutional Animal Care & Use Program (IACUC).

METHOD DETAILS

Open field test—Nitrogen gas was mixed into a 20” × 20” Photobeam Activity System (PAS)-Open Field Chamber (San Diego Instruments) to bring the F_iO_2 to the appropriate level. An O_2 gas sensor (Vernier) was used to monitor the oxygen levels in the chamber. Mice housed at 21%, 11%, and 8% F_iO_2 were moved into the chamber of matching F_iO_2 for 10 minutes. Their movement was recorded in real time with built-in photobeams and compiled with PAS-Open Field Software (San Diego Instruments).

Pole test—3–4 days prior to the test, mice were pre-trained on the 50 cm pole. Mice were placed at the top of the pole, facing up and facing down, and the time required to descend from this starting position to the bottom of the pole was measured. Each test was conducted 3 times, and the average score was calculated. For the facing down starting condition,

latency to descend was scored as follows: for mice sliding <20% of the pole, the lesser of 1.25 times the total time or 15s was recorded; for mice sliding 20–50% of the pole, 15s was recorded; for mice that fell, a max score of 20s was recorded. For the facing up starting condition, latency to descend was scored as follows: for mice sliding <20% of the pole, 1.25 times the total time was recorded; for mice sliding 20–50% of the pole, 30s was recorded; for mice sliding 50–75%, 45s was recorded; for mice sliding > 75%, 60s was recorded; for mice that fell, a max score of 75s was recorded. All experiments were conducted in a glovebox matching the appropriate F_iO_2.

Blood chemistries—Approximately 90 μL tail blood was collected from mice in a glovebox controlling the F_iO_2. Blood was collected into K2EDTA tubes (BD) and analyzed on an iSTAT handheld analyzer (Zoetis) using CHEM8+ cartridges (Zoetis).

Body temperature measurements—Mouse body temperatures were measured using an infrared camera (FLIR). Mice were imaged and the maximal observed body temperature was recorded. Temperatures were measured in a glovebox controlling the F_iO_2.

Weight and food intake measurements—Mice were weighed daily for the first week of treatment and every 2–4 days after the first week. Food intake was calculated based on the change in weight of food in cages between measurements.

Tissue oxygenation measurements—10–11-week-old male C57BL/6J mice were housed at three different conditions—21% F_iO_2, 8% F_iO_2 for 24 hours, and 8% F_iO_2 for 3 weeks. Mice were anesthetized with 4% isoflurane and endotracheally intubated using an intubation platform (Kent Scientific). After intubation, mice were placed on a flat heating pad and ventilated with the MiniVent Type 845 (Hugo Sachs Electronik, Harvard Apparatus). The stroke volume was set to 150uL and the ventilation rate was set to 150 strokes/min. During ventilation, 2% isoflurane was maintained for anesthesia.

To control the PO_2 inhaled by the ventilated mouse, pure nitrogen (>99.995%) was mixed with pure oxygen (>99.5%) using a dual flow meter (DFM-3002, Billups-Rothenberg). The nitrogen and oxygen tanks were obtained from Linde and were connected to CGA-580 and CGA-540 regulators, respectively. The outlet pressure from each regulator was set at 5 psig. The PO_2 of the gas mixture was measured by the Flow Through Oxygen Monitor (GMS-5002, Billups-Rothenberg). The nitrogen flow rate was maintained at 5 L/min and the oxygen flow rate was adjusted as needed to keep the PO_2 of the mixed gas within 0.2% of the desired F_iO_2. The outlet from the Flow Through Oxygen Monitor was then connected to the gas inlet of an isoflurane vaporizer.

In order to measure tissue oxygen tensions, a 50μm-wide Clark-type electrode (Unisense OX-50) was lowered into an exposed organ after a surgical incision was made. A micromanipulator was used to move the electrode. Measurements were recorded after readings were stable for 10 seconds. The electrode was polarized for at least 2 hours before use. For calibration, two oxygen tensions were used—room air (159.6 mmHg) bubbled into 31°C PBS, and a 31°C anoxic (0 mmHg) sodium ascorbate solution at pH 9.9 (Unisense). Using a handheld rodent thermometer with a probe (Braintree Scientific), we determined

that the intra-abdominal and intra-thoracic temperature of two dissected mice on a heating paid was approximately 30–32°C. Prior to sampling the brain, the Ideal Micro-Drill (Roboz, RS-6300A) was used to drill through the skull. The following regions were sampled in each organ: lung—right middle lobe, heart—right ventricle, eWAT—right eWAT, brain—cerebral cortex, liver—medial lobe, muscle—right quadriceps, kidney—right kidney, BAT—interscapular BAT.

Hormone measurements—Tail blood was collected from mice in a glovebox controlling the F_iO_2 and stored in K2EDTA tubes (BD). Plasma was extracted by centrifuging the blood samples at 2,000 rpm for 10 minutes at 4C and collecting the supernatant. Plasma samples were shipped on dry ice to the UC Davis mouse metabolic phenotyping core. Hormone concentrations were measured using multi-spot assay (insulin, leptin; Meso Scale Discovery), radioimmunoassay (glucagon; Millipore) (corticosterone; MP Biomedicals), or ELISA (ghrelin; Millipore).

Blood glucose measurements—Blood glucose levels were measured using a handheld glucometer (AimStrip Plus). For fasted measurements, mice were fasted overnight for 12 hours.

Radiotracers—[^{18}F]fluoride ion was produced by the ^{18}O(p,n)^{18}F reaction in the UCSF GE PETtrace™ cyclotron by proton irradiation of oxygen-18 enriched water (Rotem). FDG was prepared in the UCSF Radiopharmaceutical Facility from [^{18}F]fluoride ion by automated synthesis on the GE FASTlab synthesizer using the FDG Citrate FASTlab reagent cassette (GE). For FTP synthesis, Methyl 16-bromo-4-thia-hexadecanoate precursor (16-[^{18}F]fluoro-4-thia-hexadecanoic acid) was synthesized from 1,12 dibromododecane following previously reported methods.[55] FTP was prepared by reacting the methyl hexadecanoate precursor with [^{18}F]fluoride ion followed by saponification of the methyl ester and HPLC purification.

Mouse PET scans and gamma counting—Mouse PET/CT scans (Inveon, Siemens Medical Solutions) were conducted at the Preclinical Imaging Core facility at China Basin in the UCSF Department of Radiology & Biomedical Imaging. Mice were transported in boxes and transportable N_2 and O_2 tanks (Airgas) were used to maintain the appropriate F_iO_2 in transit. Mice were anesthetized with isoflurane and administered FDG or FTP via tail vein injections. After 30 minutes, the mice were anesthetized and positioned for PET/CT scan. After completion of the scan, mice were euthanized and organs were harvested. Organs were either imaged using the microPET/CT scanner or entered into a gamma counter (HIDEX Automatic Gamma Counter) for quantification of the radioactivity, which was normalized based on organ weight and dose at scan-time. The percent injected dose per gram was calculated for blood and tissues. Dose at the time of scanning or counting was decay-corrected using the known half-life of the radionuclide used for imaging according to the following equation, with Δt representing the time between injection and scan:

$$Dose_{scan/count} = Dose_{injection}\left(e^{\frac{-\Delta t \times \ln(2)}{109.771}}\right)$$

All measured values from microPET/CT and gamma counting were calibrated to quantitatively represent physical activity levels using routine calibration methods employed for both. Images were viewed using AMIDE.[73]

Organ and blood collection—10–11-week-old male C57BL/6J mice were housed at three different conditions—21% F_iO_2, 8% F_iO_2 for 24 hours, and 8% F_iO_2 for 3 weeks. Mice were briefly anesthetized with isoflurane, and blood was collected using cardiac puncture. Next, mice were euthanized by isoflurane overdose. For each mouse, the systemic circulation was perfused with PBS by cutting the right atrium and inserting into the left ventricle a needle connected to a peristaltic perfusion pump (Fisher Scientific). After perfusion for 2 minutes, approximately 50–100 mg of each organ was collected and stored in 500 μL RNAlater (Thermo Fisher Scientific). Organ samples in RNAlater were stored overnight at −20°C and then moved to −80°C.

RNA extraction—Organs were transferred from RNAlater solution to 1 mL Trizol. A stainless-steel bead (Qiagen) was added to each sample before lysing in a tissue lyser (Qiagen) for three 1-minute cycles at a frequency of 30 Hz. Samples were incubated at room temperature for 5 minutes, then 250 μL of chloroform was added and mixed. After another 5-minute incubation at room temperature, samples were centrifuged at 10,000 rpm for 10 minutes at 4°C. 400 μL of the aqueous layer was collected and mixed with 500 μL isopropanol. After incubating at room temperature for 5 minutes, samples were centrifuged at 15,000 rpm for 30 minutes at 4°C. Samples were placed on ice, and the supernatant was removed. 1 mL of 75% ethanol was added before centrifuging at 9500 rpm for 5 minutes at 4°C. After supernatant was removed, 1 mL of 75% ethanol was added, and samples were centrifuged at 9500 rpm for 5 minutes at 4°C. Following the removal of supernatant, 20–100 μL DEPC water was added, depending on the size of the pellet. Samples were incubated in a 60°C heat block for 10 minutes or until the pellet dissolved. RNA concentration and quality was determined using a NanoDrop 2000c spectrophotometer (Thermo Fisher Scientific).

RT-PCR—RNA was reverse transcribed to cDNA using the QuantiTect Reverse Transcription Kit (Qiagen). 2 μL of gDNA wipeout buffer was added to a 12 μL solution of RNA in water containing approximately 1 μg of RNA. Samples were incubated at 42°C for 2 minutes before placing on ice. Next, 1 μL reverse transcriptase, 1 μL RT primer mix, and 4 μL 5X RT buffer were added to each sample. Samples were incubated at 42°C for 15 minutes and 95°C for 3 minutes. Resulting cDNA was stored at −20°C.

For each qPCR reaction, 12 μL Maxima SYBR Green/ROX qPCR Master Mix (Thermo Fisher Scientific) was mixed with 6.8 μL water, 0.6 μL each of forward and reverse primers (0.3 μM in final solution) (Table S1), and .9 μL of cDNA in a well of a 384-well plate. Each sample was run in duplicate. The plate was then inserted into a QuantStudio 5 (Applied Biosystems, Thermo Fisher Scientific) for determination of cycle threshold (CT) values. The following thermal cycle was used: 50°C for 2 minutes, 95°C for 10 minutes, then 40 cycles of 95°C for 15 seconds and 60°C for 1 minute, followed by 95°C for 15 seconds, 60°C for 1 minute, and 95°C for 15 seconds. For each set of duplicates, an average CT value was collected, and the difference in average CT between the target gene and β-actin was calculated (ΔCT). Next, the difference in ΔCT value between each sample and the average

of the normoxia samples was calculated (ΔΔCT). Relative expression of each gene was determined by calculating $2^{-\Delta\Delta CT}$.

***In vivo* ^{13}C-labeled fuel tracer experiments—**Mice were injected with approximately 1mg/g U-^{13}C-glucose (Cambridge Isotope Laboratories) or .018 mg/g U-^{13}C-palmitic acid (Sigma Aldrich). U-^{13}C-glucose doses were dissolved in water and U-^{13}C-palmitic acid was conjugated with bovine serum albumin (BSA, 35% water solution) with a PA:BSA molar ratio of 2.65:1. Mice were briefly anesthetized with isoflurane and delivered 100 μL of the tracer through retro-orbital injections. After 20, 45, or 90 minutes, blood was collected using cardiac puncture and stored in K2EDTA tubes (BD). Mice were then euthanized by cervical dislocation, and organs were harvested and flash frozen in liquid nitrogen.

Metabolite extraction—Plasma was extracted from blood by centrifuging at 2,000 rpm for 10 minutes at 4C and collecting supernatant. For tracer experiments, plasma metabolites were extracted by adding 65 μL of 80% methanol to every 5 μL of plasma. Samples were vortexed for 10s and incubated at 4°C for 10 minutes. Next, samples were centrifuged at 16,000g for 10 minutes at 4°C and supernatant was collected.

For organs, 10 μL methanol and 8 μL water were added for every 1 mg of tissue harvested. A stainless-steel bead (Qiagen) was added to each tube, and samples were lysed by undergoing five 30s on-off cycles in a tissue lyser (Qiagen) at a frequency of 30 Hz. Next, beads were removed and 10 μL chloroform was added for every 1 mg of tissue harvested. Samples were centrifuged at 14,000 rpm for 10 minutes, and the top layer (aqueous) was stored.

LC-MS—Samples were run on an Orbitrap Exploris 240 high resolution mass spectrometer (HRMS, Thermo Fisher Scientific) using electrospray ionization. The OE240 was coupled to hydrophilic interaction chromatography on a Vanquish Horizon ultra-high performance liquid chromatography (UHPLC, Thermo Fisher Scientific). 5 μLof polar metabolite samples were injected into the LC-MS system and separated on a BEH-Amide column (Waters, 2.1mm × 150mm). The autosampler was maintained at 4°C and the column was maintained at 45°C during runs. Mobile phase A was 20 mM ammonium acetate in 95:5 water:acetonitrile, with ammonium hydroxide added to reach a pH of 9.45. Mobile phase B was acetonitrile. Flow rate was 150 μL/min. The gradient was the following: 0–20 min: 80% B to 20% B; 20–20.5 min: linear gradient from 20–80% B; 20.5–28 min: stable at 80% B.[74] A 3-minute equilibration phase was included at starting conditions before each injection. The OE240 ran in full-scan, negative mode with an ion voltage of 3.0 kV, and the scan range was 70–1000 m/z. The orbitrap resolution was 60000, RF Lens was 50%, AGC target was 1e6, and the maximum injection time was 20 ms. The sheath gas was set to 40 units, auxiliary gas was 15 units, and sweep gas was 1 unit. The ion transfer tube temperature was 275°C, and the vaporizer temperature was 320°C.

QUANTIFICATION AND STATISTICAL ANALYSIS

LC-MS data analysis—Peaks were detected and peak areas were quantified using TraceFinder 5.1 General Quan. Natural isotope abundance correction was conducted using

the R package AccuCor.[75] Next, relative enrichment of the isotope label was calculated for each metabolite by determining the proportion of carbons that were ^{13}-C-labeled. No isotopomers of TCA metabolites were excluded from analysis because all can plausibly emerge from oxidative metabolism of circulating fuels (Fig S4A). For all organ data, relative enrichments of TCA metabolites were normalized to the relative enrichment of circulating glucose or palmitate (Fig S5B).

Relative enrichment was calculated according to the following formula:

$$Relative\ Enrichment = \frac{1}{nP}\sum_{n}^{i=0} i * abundance_{m+i}$$

where n represents the total carbons in a compound (4 for malate), P represents the total abundance of the compound, and m+i refers to the possible isotopomers (e.g. m+1 labeling implies one carbon is labeled). Normalized relative enrichment was calculated by dividing the relative enrichment of the tissue TCA metabolite by the relative enrichment of the tracer (glucose or palmitate) in circulation.

The resulting normalized relative enrichment values were plotted and analyzed using GraphPad Prism. Statistical significance was determined using one-way ANOVA and post-hoc Dunnett's test for multiple comparisons to a control group.

Statistical analysis

For analysis of LC-MS, qPCR, and tissue oxygenation experiments, GraphPad Prism was used. For all other data analysis and representation, R was used. Graphs were made using ggplot2.[76] Statistics were calculated using two-way ANOVA and either post-hoc Tukey test for multiple comparisons or post-hoc Dunnett's test for multiple comparisons to a control group. Exact sample sizes and statistical tests used are indicated in figure legends. Statistical significance was depicted on ggplot2 graphs using ggsignif.[77] Where used, boxplots depict the median, first quartile, and third quartile.

Supplementary Material

Refer to Web version on PubMed Central for supplementary material.

ACKNOWLEDGEMENTS

We thank all members of the Jain lab and Francoise Chanut for thoughtful discussions and review of the manuscript. We thank the UC Davis Mouse Metabolic Phenotyping Core for mouse hormone concentration measurements. We thank Ryan Tang for his technical assistance with PET/CT scans and associated radiotracer injections. We acknowledge the UCSF Radiopharmaceutical Facility for providing the FDG and [^{18}F]fluoride ion for subsequent preparation of FTP. We thank Rahul Deshpande and Bashar Amer from Thermo Fisher Scientific for their technical guidance with mass spectrometry. We thank Tami Tolpa for assistance with designing the graphical abstract. ADM was supported by the National Institute of General Medical Sciences (NIGMS) Medical Scientist Training Program, Grant T32GM141323. IHJ was supported by NIH DP5OD026398. IHJ, BBQ and AMB were supported by Defense Advanced Research Projects Agency, Biological Technologies Office (BTO) Program: Panacea issued by DARPA/CMO under Cooperative Agreement No. HR0011-19-2-0018. AGH was supported by the CIRM Regenerative Medicine Research Training Program. This material is based upon work supported by the National Science Foundation Graduate Research Fellowship Program under Grant No. 2034836. Any opinions,

findings, and conclusions or recommendations expressed in this material are those of the authors and do not necessarily reflect the views of the National Science Foundation.

REFERENCES:

1. Imray C, Booth A, Wright A, and Bradwell A (2011). Acute altitude illnesses. BMJ 343, d4943. 10.1136/bmj.d4943. [PubMed: 21844157]
2. Murry CE, Jennings RB, and Reimer KA (1986). Preconditioning with ischemia: a delay of lethal cell injury in ischemic myocardium. Circulation 74, 1124–1136. 10.1161/01.cir.74.5.1124. [PubMed: 3769170]
3. Schott RJ, Rohmann S, Braun ER, and Schaper W (1990). Ischemic preconditioning reduces infarct size in swine myocardium. Circ Res 66, 1133–1142. 10.1161/01.RES.66.4.1133. [PubMed: 2317890]
4. Lankford AR, Yang J-N, Rose'Meyer R, French BA, Matherne GP, Fredholm BB, and Yang Z (2006). Effect of modulating cardiac A1 adenosine receptor expression on protection with ischemic preconditioning. American Journal of Physiology-Heart and Circulatory Physiology 290, H1469–H1473. 10.1152/ajpheart.00181.2005. [PubMed: 16299262]
5. Liu Y, and Downey JM (1992). Ischemic preconditioning protects against infarction in rat heart. Am J Physiol 263, H1107–12. 10.1152/ajpheart.1992.263.4.H1107. [PubMed: 1415759]
6. Carr CS, Hill RJ, Masamune H, Kennedy SP, Knight DR, Tracey WR, and Yellon DM (1997). Evidence for a role for both the adenosine A1 and A3 receptors in protection of isolated human atrial muscle against simulated ischaemia. Cardiovasc Res 36, 52–59. 10.1016/s0008-6363(97)00160-0. [PubMed: 9415272]
7. Gho BC, Schoemaker RG, van den Doel MA, Duncker DJ, and Verdouw PD (1996). Myocardial protection by brief ischemia in noncardiac tissue. Circulation 94, 2193–2200. 10.1161/01.cir.94.9.2193. [PubMed: 8901671]
8. Olenchock BA, Moslehi J, Baik AH, Davidson SM, Williams J, Gibson WJ, Chakraborty AA, Pierce KA, Miller CM, Hanse EA, et al. (2016). EGLN1 Inhibition and Rerouting of α-Ketoglutarate Suffice for Remote Ischemic Protection. Cell 164, 884–895. 10.1016/j.cell.2016.02.006. [PubMed: 26919427]
9. Jaakkola P, Mole DR, Tian YM, Wilson MI, Gielbert J, Gaskell SJ, von Kriegsheim A, Hebestreit HF, Mukherji M, Schofield CJ, et al. (2001). Targeting of HIF-alpha to the von Hippel-Lindau ubiquitylation complex by O2-regulated prolyl hydroxylation. Science 292, 468–472. 10.1126/science.1059796. [PubMed: 11292861]
10. Epstein AC, Gleadle JM, McNeill LA, Hewitson KS, O'Rourke J, Mole DR, Mukherji M, Metzen E, Wilson MI, Dhanda A, et al. (2001). C. elegans EGL-9 and mammalian homologs define a family of dioxygenases that regulate HIF by prolyl hydroxylation. Cell 107, 43–54. 10.1016/s0092-8674(01)00507-4. [PubMed: 11595184]
11. Ivan M, Kondo K, Yang H, Kim W, Valiando J, Ohh M, Salic A, Asara JM, Lane WS, and Kaelin WG Jr. (2001). HIFα Targeted for VHL-Mediated Destruction by Proline Hydroxylation: Implications for O 2 Sensing. Science 292, 464–468. 10.1126/science.1059817. [PubMed: 11292862]
12. Haase VH (2013). Regulation of erythropoiesis by hypoxia-inducible factors. Blood Rev 27, 41–53. 10.1016/j.blre.2012.12.003. [PubMed: 23291219]
13. Pugh CW, and Ratcliffe PJ (2003). Regulation of angiogenesis by hypoxia: role of the HIF system. Nat Med 9, 677–684. 10.1038/nm0603-677. [PubMed: 12778166]
14. Tremblay JC, and Ainslie PN (2021). Global and country-level estimates of human population at high altitude. Proceedings of the National Academy of Sciences 118. 10.1073/pnas.2102463118.
15. Dünnwald T, Gatterer H, Faulhaber M, Arvandi M, and Schobersberger W (2019). Body Composition and Body Weight Changes at Different Altitude Levels: A Systematic Review and Meta-Analysis. Front Physiol 10. 10.3389/fphys.2019.00430.
16. Voss JD, Allison DB, Webber BJ, Otto JL, and Clark LL (2014). Lower Obesity Rate during Residence at High Altitude among a Military Population with Frequent Migration: A Quasi Experimental Model for Investigating Spatial Causation. PLoS One 9, e93493. 10.1371/journal.pone.0093493. [PubMed: 24740173]

17. Díaz-Gutiérrez J, Martínez-González MÁ, Pons Izquierdo JJ, González-Muniesa P, Martínez JA, and Bes-Rastrollo M (2016). Living at Higher Altitude and Incidence of Overweight/Obesity: Prospective Analysis of the SUN Cohort. PLoS One 11, e0164483. 10.1371/journal.pone.0164483. [PubMed: 27812092]

18. Merrill RM (2020). Explaining the Inverse Association between Altitude and Obesity. J Obes 2020, 1–8. 10.1155/2020/1946723.

19. Xu S, Wang Q, Liu J, Bian B, Yu X, Yu X, Ning X, and Wang J (2017). The prevalence of and risk factors for diabetes mellitus and impaired glucose tolerance among Tibetans in China: a cross-sectional study. Oncotarget 8, 112467–112476. 10.18632/oncotarget.21301. [PubMed: 29348840]

20. Koufakis T, Karras SN, Mustafa OG, Zebekakis P, and Kotsa K (2019). The Effects of High Altitude on Glucose Homeostasis, Metabolic Control, and Other Diabetes-Related Parameters: From Animal Studies to Real Life. High Alt Med Biol 20, 1–11. 10.1089/ham.2018.0076. [PubMed: 30362832]

21. Castillo O, Woolcott OO, Gonzales E, Tello V, Tello L, Villarreal C, Méndez N, Damas L, and Florentini E (2007). Residents at High Altitude Show a Lower Glucose Profile Than Sea-Level Residents Throughout 12-Hour Blood Continuous Monitoring. High Alt Med Biol 8, 307–311. 10.1089/ham.2007.8407. [PubMed: 18081506]

22. Lopez-Pascual A, Arévalo J, Martínez JA, and González-Muniesa P (2018). Inverse Association Between Metabolic Syndrome and Altitude: A Cross-Sectional Study in an Adult Population of Ecuador. Front Endocrinol (Lausanne) 9, 658. 10.3389/fendo.2018.00658. [PubMed: 30483215]

23. Lopez-Pascual A, Bes-Rastrollo M, Sayón-Orea C, Perez-Cornago A, Díaz-Gutiérrez J, Pons JJ, Martínez-González MA, González-Muniesa P, and Martínez JA (2016). Living at a Geographically Higher Elevation Is Associated with Lower Risk of Metabolic Syndrome: Prospective Analysis of the SUN Cohort. Front Physiol 7, 658. 10.3389/fphys.2016.00658. [PubMed: 28101063]

24. Ortiz-Prado E, Espinosa PS, Borrero A, Cordovez SP, Vasconez JE, Barreto-Grimales A, Coral-Almeida M, Henriquez-Trujillo AR, Simbaña-Rivera K, Gomez-Barreno L, et al. (2021). Stroke-Related Mortality at Different Altitudes: A 17-Year Nationwide Population-Based Analysis From Ecuador. Front Physiol 12. 10.3389/fphys.2021.733928.

25. Baibas N, Trichopoulou A, Voridis E, and Trichopoulos D (2005). Residence in mountainous compared with lowland areas in relation to total and coronary mortality. A study in rural Greece. J Epidemiol Community Health 59, 274–278. 10.1136/jech.2004.025510. [PubMed: 15767379]

26. Faeh D, Gutzwiller F, Bopp M, and Swiss National Cohort Study Group (2009). Lower mortality from coronary heart disease and stroke at higher altitudes in Switzerland. Circulation 120, 495–501. 10.1161/CIRCULATIONAHA.108.819250. [PubMed: 19635973]

27. Auvinen J, Tapio J, Karhunen V, Kettunen J, Serpi R, Dimova EY, Gill D, Soininen P, Tammelin T, Mykkänen J, et al. (2021). Systematic evaluation of the association between hemoglobin levels and metabolic profile implicates beneficial effects of hypoxia. Sci Adv 7. 10.1126/sciadv.abi4822.

28. Jain IH, Zazzeron L, Goli R, Alexa K, Schatzman-Bone S, Dhillon H, Goldberger O, Peng J, Shalem O, Sanjana NE, et al. (2016). Hypoxia as a therapy for mitochondrial disease. Science 352, 54–61. 10.1126/science.aad9642. [PubMed: 26917594]

29. Lewis GD, Farrell L, Wood MJ, Martinovic M, Arany Z, Rowe GC, Souza A, Cheng S, McCabe EL, Yang E, et al. (2010). Metabolic signatures of exercise in human plasma. Sci Transl Med 2, 33ra37. 10.1126/scitranslmed.3001006.

30. Steinhauser ML, Olenchock BA, O'Keefe J, Lun M, Pierce KA, Lee H, Pantano L, Klibanski A, Shulman GI, Clish CB, et al. (2018). The circulating metabolome of human starvation. JCI Insight 3. 10.1172/jci.insight.121434.

31. al Tameemi W, Dale TP, Al-Jumaily RMK, and Forsyth NR (2019). Hypoxia-Modified Cancer Cell Metabolism. Front Cell Dev Biol 7. 10.3389/fcell.2019.00004.

32. Solaini G, Baracca A, Lenaz G, and Sgarbi G (2010). Hypoxia and mitochondrial oxidative metabolism. Biochimica et Biophysica Acta (BBA) - Bioenergetics 1797, 1171–1177. 10.1016/j.bbabio.2010.02.011. [PubMed: 20153717]

33. Eales KL, Hollinshead KER, and Tennant DA (2016). Hypoxia and metabolic adaptation of cancer cells. Oncogenesis 5, e190–e190. 10.1038/oncsis.2015.50. [PubMed: 26807645]

34. Balkaya M, and Endres M (2010). Behavioral Testing in Mouse Models of Stroke. In Rodent Models of Stroke. Neuromethods, Dirnagl U, ed. (Humana Press), pp. 179–197. 10.1007/978-1-60761-750-1_13.

35. Lawrence JH, Huff RL, Siri W, Wasserman LR, and Hennessy TG (1952). A physiological study in the Peruvian Andes. Acta Med Scand 142, 117–131. 10.1111/j.0954-6820.1952.tb13851.x. [PubMed: 14932785]

36. Pugh LG (1964). Blood Volume and Haemoglobin Concentration at Altitudes Above 18,000 Ft. (5500 M). J Physiol 170, 344–354. 10.1113/jphysiol.1964.sp007335. [PubMed: 14165170]

37. Gautier H, Bonora M, M'Barek SB, and Sinclair JD (1991). Effects of hypoxia and cold acclimation on thermoregulation in the rat. J Appl Physiol 71, 1355–1363. 10.1152/jappl.1991.71.4.1355. [PubMed: 1757358]

38. Kuhnen G, Wloch B, and Wünnenberg W (1987). Effects of acute hypoxia and/or hypercapnia on body temperatures and cold induced thermogenesis in the golden hamster. J Therm Biol 12, 103–107. 10.1016/0306-4565(87)90046-5.

39. Cheng H, Sebaa R, Malholtra N, Lacoste B, el Hankouri Z, Kirby A, Bennett NC, van Jaarsveld B, Hart DW, Tattersall GJ, et al. (2021). Naked mole-rat brown fat thermogenesis is diminished during hypoxia through a rapid decrease in UCP1. Nat Commun 12, 6801. 10.1038/s41467-021-27170-2. [PubMed: 34815412]

40. DiPasquale DM, Kolkhorst FW, and Buono MJ (2015). Acute normobaric hypoxia reduces body temperature in humans. High Alt Med Biol 16, 61–66. 10.1089/ham.2014.1098. [PubMed: 25803142]

41. Wood SC (1991). Interactions between hypoxia and hypothermia. Annu Rev Physiol 53, 71–85. 10.1146/annurev.ph.53.030191.000443. [PubMed: 2042977]

42. Reinboth BS, Köster C, Abberger H, Prager S, Bendix I, Felderhoff-Müser U, and Herz J (2016). Endogenous hypothermic response to hypoxia reduces brain injury: Implications for modeling hypoxic-ischemic encephalopathy and therapeutic hypothermia in neonatal mice. Exp Neurol 283, 264–275. 10.1016/j.expneurol.2016.06.024. [PubMed: 27349408]

43. Abu Eid S, Hackl MT, Kaplanian M, Winter M-P, Kaltenecker D, Moriggl R, Luger A, Scherer T, and Fürnsinn C (2018). Life Under Hypoxia Lowers Blood Glucose Independently of Effects on Appetite and Body Weight in Mice. Front Endocrinol (Lausanne) 9. 10.3389/fendo.2018.00490.

44. Shukla V, Singh SN, Vats P, Singh VK, Singh SB, and Banerjee PK (2005). Ghrelin and leptin levels of sojourners and acclimatized lowlanders at high altitude. Nutr Neurosci 8, 161–165. 10.1080/10284150500132823. [PubMed: 16117183]

45. Vats P, Singh SN, Shyam R, Singh VK, Singh SB, Banerjee PK, and Selvamurthy W (2004). Leptin may not be responsible for high altitude anorexia. High Alt Med Biol 5, 90–92. 10.1089/152702904322963753. [PubMed: 15072723]

46. Morishima T, and Goto K (2016). Ghrelin, GLP-1, and leptin responses during exposure to moderate hypoxia. Appl Physiol Nutr Metab 41, 375–381. 10.1139/apnm-2015-0311. [PubMed: 26863323]

47. Giesecke K, Magnusson I, Ahlberg M, Hagenfeldt L, and Wahren J (1989). Protein and amino acid metabolism during early starvation as reflected by excretion of urea and methylhistidines. Metabolism 38, 1196–1200. 10.1016/0026-0495(89)90159-5. [PubMed: 2593832]

48. Hoppeler H, Kleinert E, Schlegel C, Claassen H, Howald H, Kayar SR, and Cerretelli P (1990). Morphological adaptations of human skeletal muscle to chronic hypoxia. Int J Sports Med 11 Suppl 1, S3–9. 10.1055/s-2007-1024846. [PubMed: 2323861]

49. MacDougall JD, Green HJ, Sutton JR, Coates G, Cymerman A, Young P, and Houston CS (1991). Operation Everest II: structural adaptations in skeletal muscle in response to extreme simulated altitude. Acta Physiol Scand 142, 421–427. 10.1111/j.1748-1716.1991.tb09176.x. [PubMed: 1927554]

50. Frezza C, Zheng L, Tennant DA, Papkovsky DB, Hedley BA, Kalna G, Watson DG, and Gottlieb E (2011). Metabolic profiling of hypoxic cells revealed a catabolic signature required for cell survival. PLoS One 6, e24411. 10.1371/journal.pone.0024411. [PubMed: 21912692]

51. Gallagher BM, Fowler JS, Gutterson NI, MacGregor RR, Wan CN, and Wolf AP (1978). Metabolic trapping as a principle of oradiopharmaceutical design: some factors resposible for

the biodistribution of [18F] 2-deoxy-2-fluoro-D-glucose. J Nucl Med 19, 1154–1161. [PubMed: 214528]

52. Zhao J, Tan C, Imai R, Ukon N, Shimoyama S, Maejima Y, Omiya Y, Takahashi K, Ito H, Nan G, et al. (2021). Evaluation of organ glucose metabolism by 18F-FDG accumulation with insulin loading in aged mice compared with young normal mice. Sci Rep 11, 7421. 10.1038/s41598-021-86825-8. [PubMed: 33795778]
53. Ryder JW, Chibalin AV, and Zierath JR (2001). Intracellular mechanisms underlying increases in glucose uptake in response to insulin or exercise in skeletal muscle. Acta Physiol Scand 171, 249–257. 10.1046/j.1365-201x.2001.00827.x. [PubMed: 11412137]
54. Betz MJ, and Enerbäck S (2018). Targeting thermogenesis in brown fat and muscle to treat obesity and metabolic disease. Nat Rev Endocrinol 14, 77–87. 10.1038/nrendo.2017.132. [PubMed: 29052591]
55. DeGrado TR, Wang S, Holden JE, Nickles RJ, Taylor M, and Stone CK (2000). Synthesis and preliminary evaluation of (18)F-labeled 4-thia palmitate as a PET tracer of myocardial fatty acid oxidation. Nucl Med Biol 27, 221–231. 10.1016/s0969-8051(99)00101-8. [PubMed: 10832078]
56. DeGrado TR, Kitapci MT, Wang S, Ying J, and Lopaschuk GD (2006). Validation of 18F-fluoro-4-thia-palmitate as a PET probe for myocardial fatty acid oxidation: effects of hypoxia and composition of exogenous fatty acids. J Nucl Med 47, 173–181. [PubMed: 16391202]
57. Su X, and Abumrad NA (2009). Cellular fatty acid uptake: a pathway under construction. Trends in Endocrinology & Metabolism 20, 72–77. 10.1016/j.tem.2008.11.001. [PubMed: 19185504]
58. Du W, Zhang L, Brett-Morris A, Aguila B, Kerner J, Hoppel CL, Puchowicz M, Serra D, Herrero L, Rini BI, et al. (2017). HIF drives lipid deposition and cancer in ccRCC via repression of fatty acid metabolism. Nat Commun 8, 1769. 10.1038/s41467-017-01965-8. [PubMed: 29176561]
59. Liu Y, Ma Z, Zhao C, Wang Y, Wu G, Xiao J, McClain CJ, Li X, and Feng W (2014). HIF-1α and HIF-2α are critically involved in hypoxia-induced lipid accumulation in hepatocytes through reducing PGC-1α-mediated fatty acid β-oxidation. Toxicol Lett 226, 117–123. 10.1016/j.toxlet.2014.01.033. [PubMed: 24503013]
60. Papandreou I, Cairns RA, Fontana L, Lim AL, and Denko NC (2006). HIF-1 mediates adaptation to hypoxia by actively downregulating mitochondrial oxygen consumption. Cell Metab 3, 187–197. 10.1016/j.cmet.2006.01.012. [PubMed: 16517406]
61. Matheson GO, Allen PS, Ellinger DC, Hanstock CC, Gheorghiu D, McKenzie DC, Stanley C, Parkhouse WS, and Hochachka PW (1991). Skeletal muscle metabolism and work capacity: a 31P-NMR study of Andean natives and lowlanders. J Appl Physiol 70, 1963–1976. 10.1152/jappl.1991.70.5.1963. [PubMed: 1864776]
62. Vilar J, Waeckel L, Bonnin P, Cochain C, Loinard C, Duriez M, Silvestre J-S, and Lévy BI (2008). Chronic Hypoxia–Induced Angiogenesis Normalizes Blood Pressure in Spontaneously Hypertensive Rats. Circ Res 103, 761–769. 10.1161/CIRCRESAHA.108.182758. [PubMed: 18703778]
63. Zouboules SM, Lafave HC, O'Halloran KD, Brutsaert TD, Nysten HE, Nysten CE, Steinback CD, Sherpa MT, and Day TA (2018). Renal reactivity: acid-base compensation during incremental ascent to high altitude. J Physiol 596, 6191–6203. 10.1113/JP276973. [PubMed: 30267579]
64. Woolcott OO, Ader M, and Bergman RN (2015). Glucose Homeostasis During Short-term and Prolonged Exposure to High Altitudes. Endocr Rev 36, 149–173. 10.1210/er.2014-1063. [PubMed: 25675133]
65. Liu Y, Luo Q, Su Z, Xing J, Wu J, Xiang L, Huang Y, Pan H, Wu X, Zhang X, et al. (2021). Suppression of Myocardial Hypoxia-Inducible Factor-1α Compromises Metabolic Adaptation and Impairs Cardiac Function in Patients With Cyanotic Congenital Heart Disease During Puberty. Circulation 143, 2254–2272. 10.1161/CIRCULATIONAHA.120.051937. [PubMed: 33663226]
66. Inigo M, Deja S, and Burgess SC (2021). Ins and Outs of the TCA Cycle: The Central Role of Anaplerosis. Annu Rev Nutr 41, 19–47. 10.1146/annurev-nutr-120420-025558. [PubMed: 34270333]
67. Murphy MP, and Chouchani ET (2022). Why succinate? Physiological regulation by a mitochondrial coenzyme Q sentinel. Nat Chem Biol 18, 461–469. 10.1038/s41589-022-01004-8. [PubMed: 35484255]

68. Kessler G, and Friedman J (1998). Metabolism of Fatty Acids and Glucose. Circulation 98. 10.1161/circ.98.13.1350/a.

69. Owen OE, Morgan AP, Kemp HG, Sullivan JM, Herrera MG, and Cahill GF (1967). Brain Metabolism during Fasting. Journal of Clinical Investigation 46, 1589–1595. 10.1172/JCI105650. [PubMed: 6061736]

70. White CJ, Lee J, Choi J, Chu T, Scafidi S, and Wolfgang MJ (2020). Determining the Bioenergetic Capacity for Fatty Acid Oxidation in the Mammalian Nervous System. Mol Cell Biol 40. 10.1128/MCB.00037-20.

71. Patt S, Sampaolo S, Théallier-Jankó A, Tschairkin I, and Cervós-Navarro J (1997). Cerebral angiogenesis triggered by severe chronic hypoxia displays regional differences. J Cereb Blood Flow Metab 17, 801–806. 10.1097/00004647-199707000-00010. [PubMed: 9270497]

72. Silva B, Mantha OL, Schor J, Pascual A, Plaçais P-Y, Pavlowsky A, and Preat T (2022). Glia fuel neurons with locally synthesized ketone bodies to sustain memory under starvation. Nat Metab 4, 213–224. 10.1038/s42255-022-00528-6. [PubMed: 35177854]

73. Loening AM, and Gambhir SS (2003). AMIDE: A Free Software Tool for Multimodality Medical Image Analysis. Mol Imaging 2, 10.1162/15353500200303133.

74. Spinelli JB, Rosen PC, Sprenger H-G, Puszynska AM, Mann JL, Roessler JM, Cangelosi AL, Henne A, Condon KJ, Zhang T, et al. (2021). Fumarate is a terminal electron acceptor in the mammalian electron transport chain. Science (1979) 374, 1227–1237. 10.1126/science.abi7495.

75. Su X, Lu W, and Rabinowitz JD (2017). Metabolite Spectral Accuracy on Orbitraps. Anal Chem 89, 5940–5948. 10.1021/acs.analchem.7b00396. [PubMed: 28471646]

76. Wickham H (2016). ggplot2: Elegant Graphics for Data Analysis (Springer International Publishing) 10.1007/978-3-319-24277-4.

77. Ahlmann-Eltze C, and Patil I (2021). ggsignif: R Package for Displaying Significance Brackets for “ggplot2.” PsyArXiv. 10.31234/osf.io/7awm6.

Highlights

- Mice exposed to hypoxia recovered locomotor deficits over 3 weeks.
- Adaptation to hypoxia coincided with reduced blood glucose and adiposity.
- Acute hypoxia promoted glucose uptake in most organs, except brown fat and muscle.
- Chronic hypoxia caused organ-level rewiring of glucose and fatty acid metabolism.

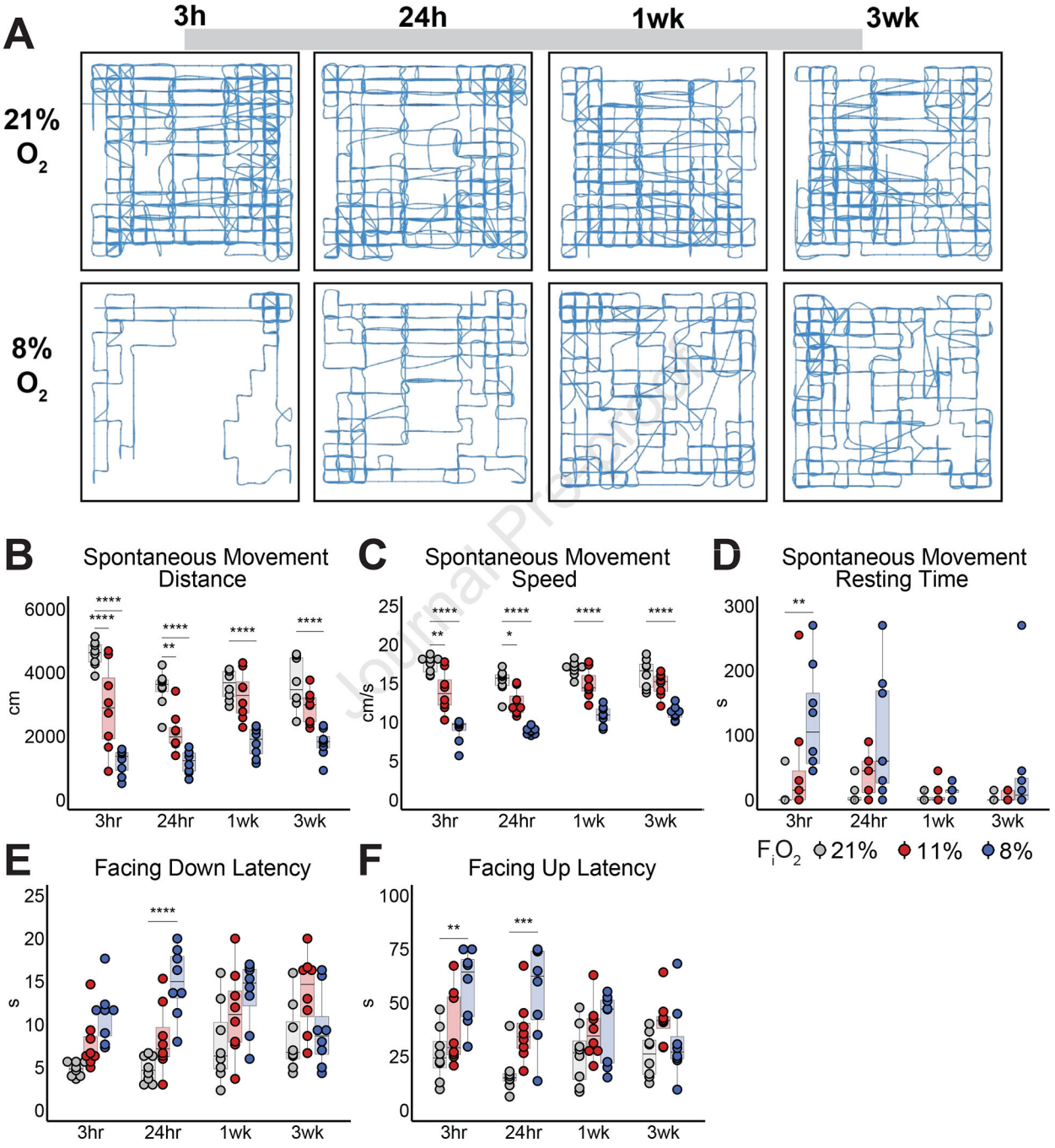

Figure 1. Acute hypoxia causes perturbations in spontaneous movement and motor coordination that attenuate over time.

(A) Representative movement traces of mice housed at 21% or 8% F_iO_2 and transferred to openfield chambers of matching F_iO_2. **(B-D) (B)** Total distance covered, **(C)** average speed, and **(D)** total resting time of mice placed in openfield chambers over 10 minutes. Mice were housed at 21% (grey), 11% (red), 8% (blue) F_iO_2 for 3 hours, 24 hours, 1 week, or 3 weeks. **(E-F)** Latency to descend (in seconds) down a pole after being placed at the top facing down

(E) or facing up **(F)**. Statistics were calculated using two-way ANOVA and post-hoc Tukey correction. N = 8 biological replicates. *p<0.5, **p<.01, ***p<.001, ****p<.0001.

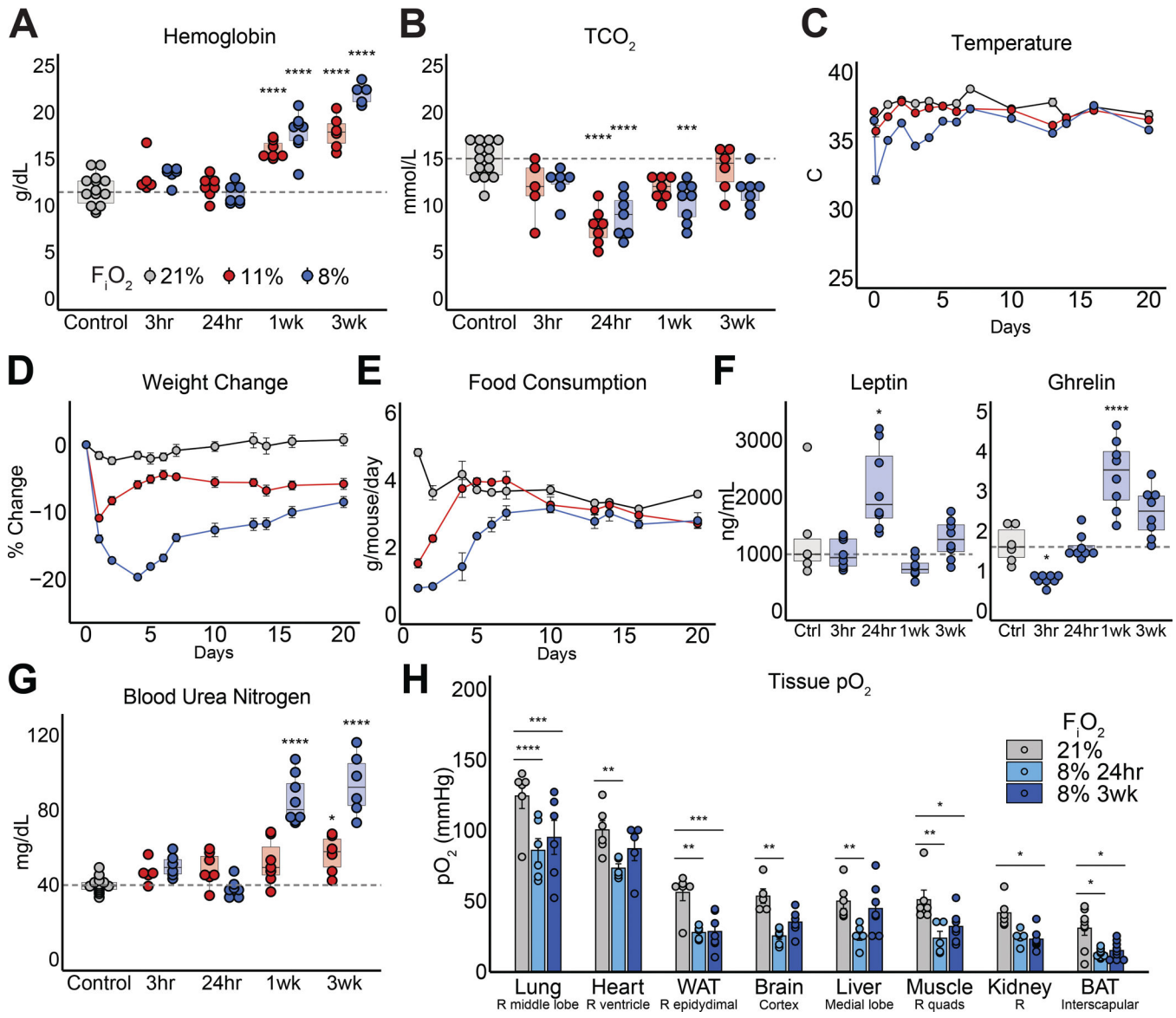

Figure 2. Physiological adaptation to hypoxia includes systemic metabolic rewiring.

(A-B) (A) Blood hemoglobin concentrations and **(B)** Total CO_2 measured from tail vein blood samples of mice housed in 21% (grey), 11% (red), or 8% F_iO_2 (blue) for 3 hours, 24 hours, 1 week, or 3 weeks. Reduced TCO_2 levels indicate hyperventilation. **(C)** Highest detectable body temperatures measured with an infrared camera daily for one week and every 2–4 days for the following 2 weeks. Mean ± SEM are shown. For 11% F_iO_2 mice, body temperatures were significantly different from normoxic mice on days 7 and 13. For 8% F_iO_2 mice, body temperatures were significantly different from normoxic mice from 3 hours to 4 days and on days 6, 7, and 13. **(D)** Percent change in body weight from baseline. Mean ± SEM are shown. For 11% F_iO_2 mice, differences in body weight change were statistically significant from day 1 to 4 and from day 7 to 20 when compared to normoxic mice. For 8% F_iO_2 mice, differences in body weight change were statistically significant from day 1 to 20 when compared to normoxic mice. **(E)** Food consumption

per mouse per day. N = 2 cages. Mean ± SEM are shown. For 11% F_iO_2 mice, food consumption was significantly different from normoxic mice on days 1 and 2. For 8% F_iO_2 mice, food consumption was significantly different from normoxic mice from day 1 to 5. **(F)** Unfasted plasma levels of leptin and ghrelin from tail blood samples collected from mice housed at 21% F_iO_2 or from mice housed at 8% F_iO_2 for 3 hours, 24 hours, 1 week, or 3 weeks. **(G)** Blood urea nitrogen (BUN) concentrations measured from tail blood samples. Elevated BUN provides evidence of increased protein degradation. **(H)** Organ-level partial pressures of oxygen measured by a Clark-type microsensor. When compared to normoxia (grey), all organs exhibited a decreased oxygen tension when exposed to acute hypoxia (light blue), and some experienced a recovery in chronic hypoxia (dark blue). N = 5–9 biological replicates. Mean ± SEM are shown. For (A)-(F), statistics were calculated using two-way ANOVA and post-hoc Tukey correction. For (G), statistics were calculated using two-way ANOVA and post-hoc Dunnett's test for multiple comparisons to a control group. N = 8 biological replicates for all panels except (E) and (G). *p<0.5, **p<.01, ***p<.001, ****p<.0001.

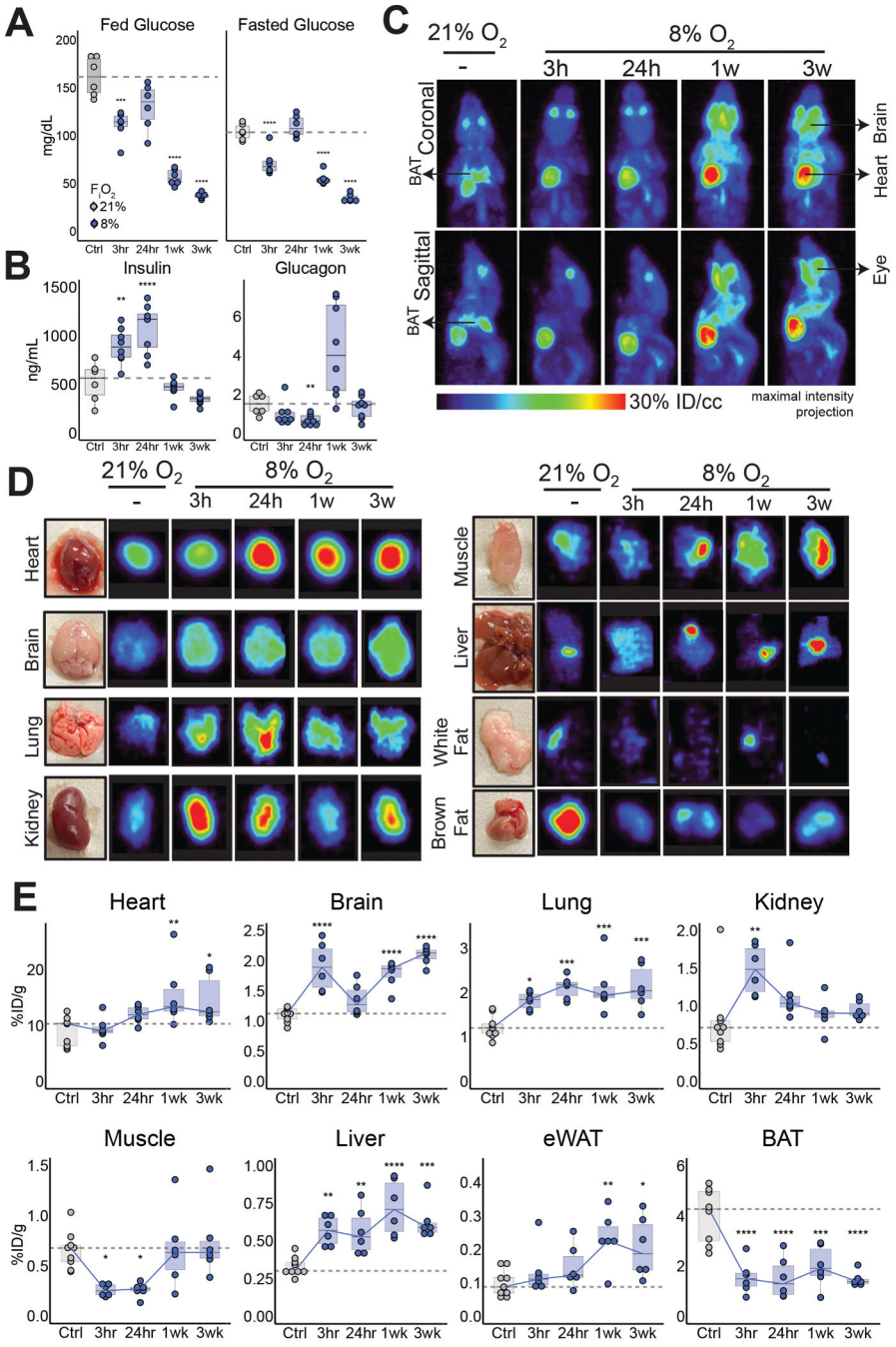

Figure 3. Chronic hypoxia causes hypoglycemia and alters organ-specific glucose uptake.

(A) Fed and fasted blood glucose measurements after 3 hours, 24 hours, 1 week, and 3 weeks of hypoxia (8% F_iO_2) treatment (blue). Controls (grey) were housed in 21% F_iO_2. **(B)** Unfasted plasma levels of insulin and glucagon from tail blood samples collected from mice housed at 21% F_iO_2 or from mice housed at 8% F_iO_2 for 3 hours, 24 hours, 1 week, or 3 weeks. **(C)** Representative coronal and sagittal images of mouse PET scans conducted 30 minutes after tail vein injection of the glucose analogue 2-Deoxy-2-[^{18}F]fluoro-D-glucose (FDG). **(D)** Representative PET scan images of organs extracted from mice 60 minutes after

tail vein injection of FDG. Maximum values (% ID/cc) vary per organ: Heart: 40, Brain: 20, Lung: 10, Kidney: 5, Muscle: 7, Liver: 7, White Fat: 2, Brown Fat: 10. **(E)** Radioactive signal from each organ after extraction as measured by a gamma counter. Values were decay-corrected based on the time of FDG injection and the time of measurement. N = 6–9 biological replicates. Statistics were calculated using one-way ANOVA and post-hoc Tukey correction. *p<0.5, **p<.01, ***p<.001, ****p<.0001. eWAT: epididymal white adipose tissue, BAT: brown adipose tissue.

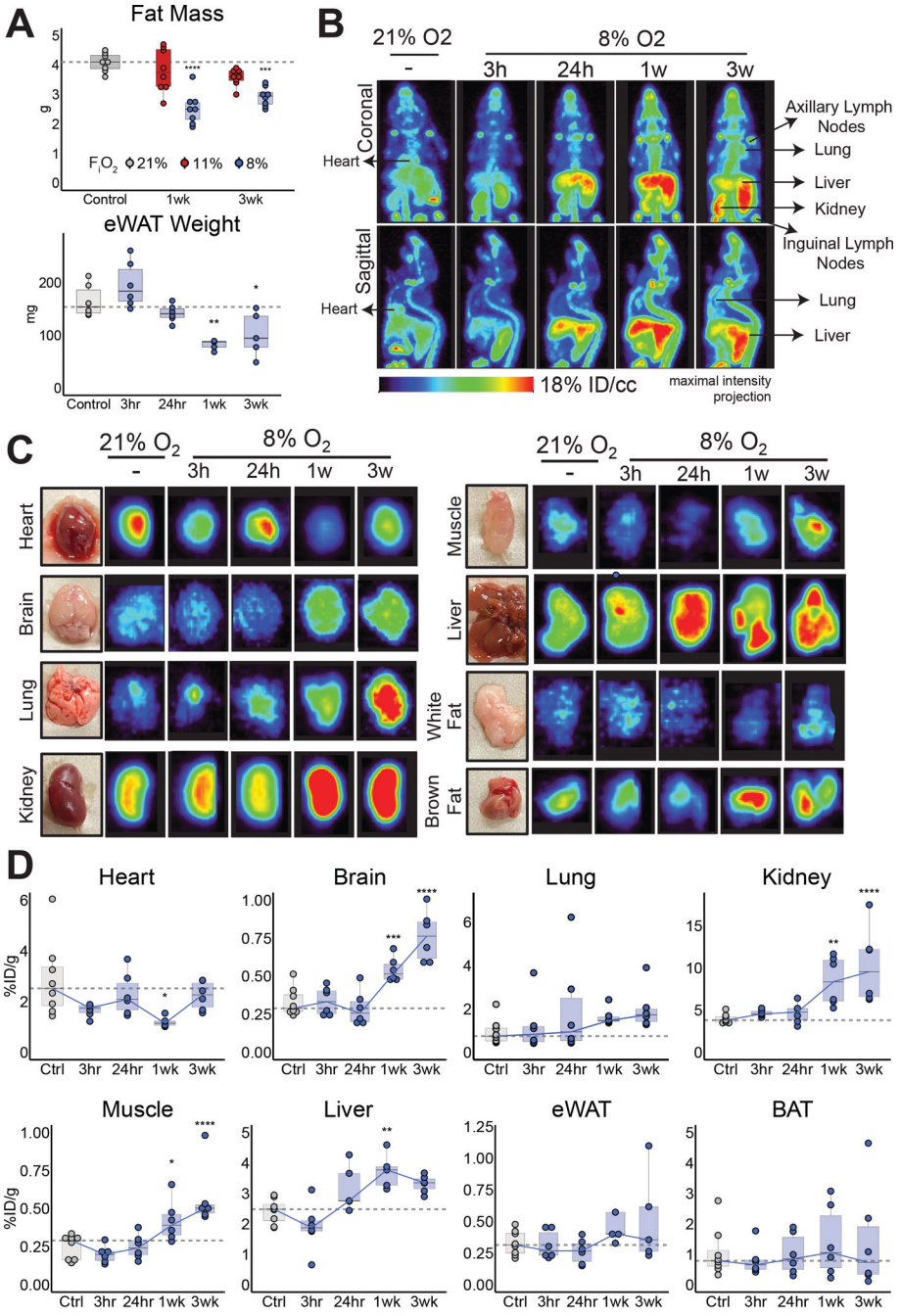

Figure 4. Chronic hypoxia reduces lipid accumulation and alters organ-specific free fatty acid uptake.

(A) Fat mass measured by DEXA scan and weights of eWAT depots in mice housed at 21% (grey), 11% (red), and 8% (blue) F_iO_2. **(B)** Representative coronal and sagittal images of mouse PET scans conducted 30 minutes after tail vein injection of the palmitate analogue 18-[18F]fluoro-4-thia-palmitate (FTP). **(C)** Representative PET scan images of organs extracted from mice 60 minutes after tail vein injection of FTP. Maximum values (% ID/cc) vary per organ: Heart: 20, Brain: 20, Lung: 20, Kidney: 50, Muscle: 7, Liver: 65, White

Fat: 2, Brown Fat: 15. **(D)** Radioactive signal from each organ after extraction as measured by a gamma counter. Values were decay-corrected based on the time of FDG injection and the time of measurement. N = 4–8 biological replicates. Statistics were calculated using one-way ANOVA and post-hoc Tukey correction. *p<0.5, **p<.01, ***p<.001, ****p<.0001. eWAT: epididymal white adipose tissue, BAT: brown adipose tissue.

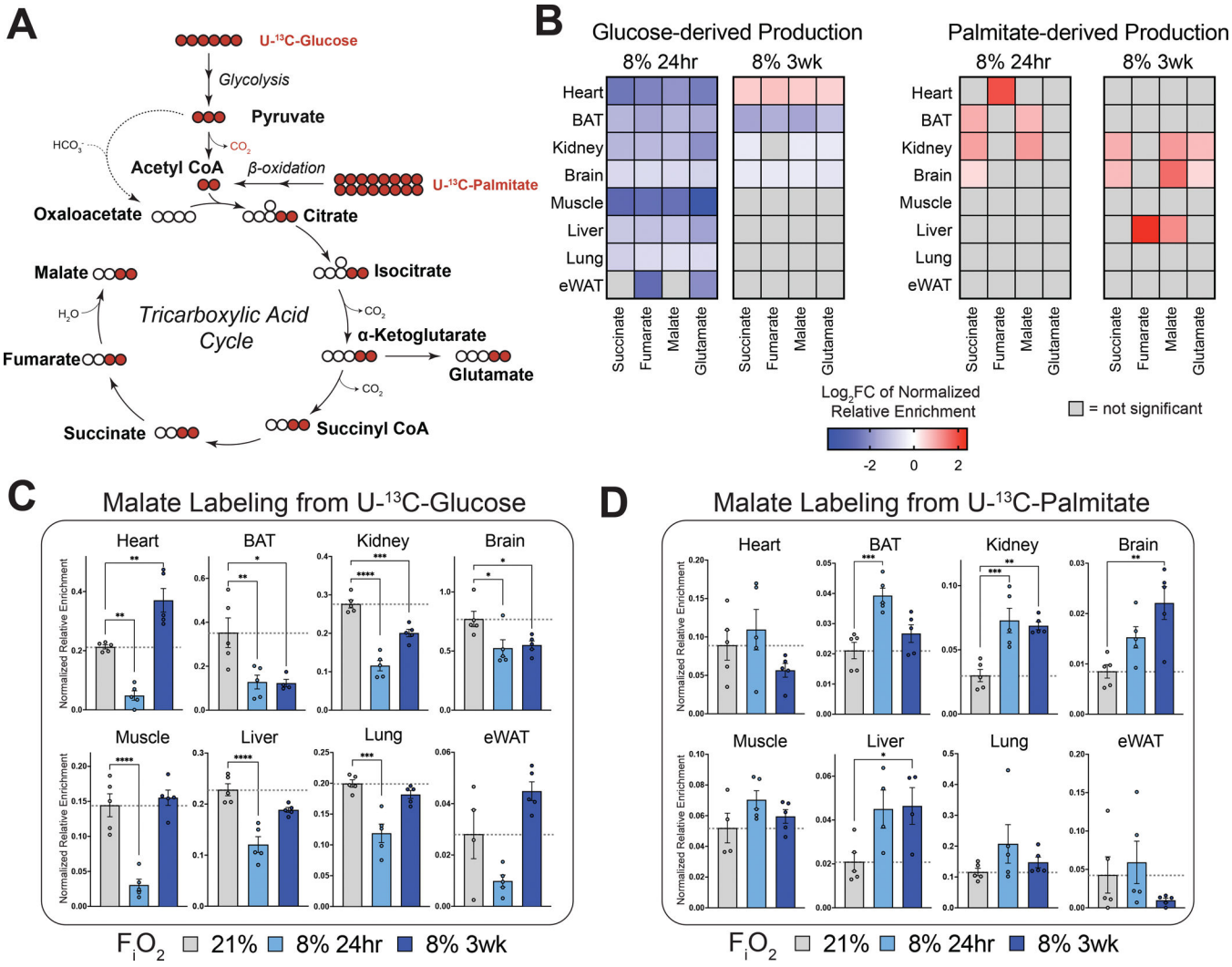

Figure 5. Hypoxia rewires metabolic flux of major fuel sources into the TCA cycle

(A) Schematic showing entry of carbons from glucose and palmitate to the TCA cycle. Red circles represent ^{13}C-labeled carbons. Labeling patterns correspond to ^{13}C-Acetyl CoA passing through one round of the TCA cycle. **(B)** Heatmap showing the median log fold change in normalized relative enrichment of the isotope label compared to the 21% F_iO_2 condition. Normalized relative enrichment was calculated by determining the fraction of carbons in TCA metabolites that were ^{13}C-labeled and subsequently normalizing to the ^{13}C enrichment of the fuel (glucose or palmitate) in plasma. Greater normalized relative enrichment indicates increased production of the target metabolite from the injected tracer compared to other sources. Only statistically significant changes are shown. **(C-D)** Normalized relative enrichment of malate 20 minutes after injection with **(C)** ^{13}C-glucose or **(D)** ^{13}C-palmitate. Mean ± SEM are shown. Statistics were calculated using one-way ANOVA and post-hoc Dunnett's test for multiple comparisons to a control group. N=4–5 biological replicates. *p<0.5, **p<.01, ***p<.001, ****p<.0001.

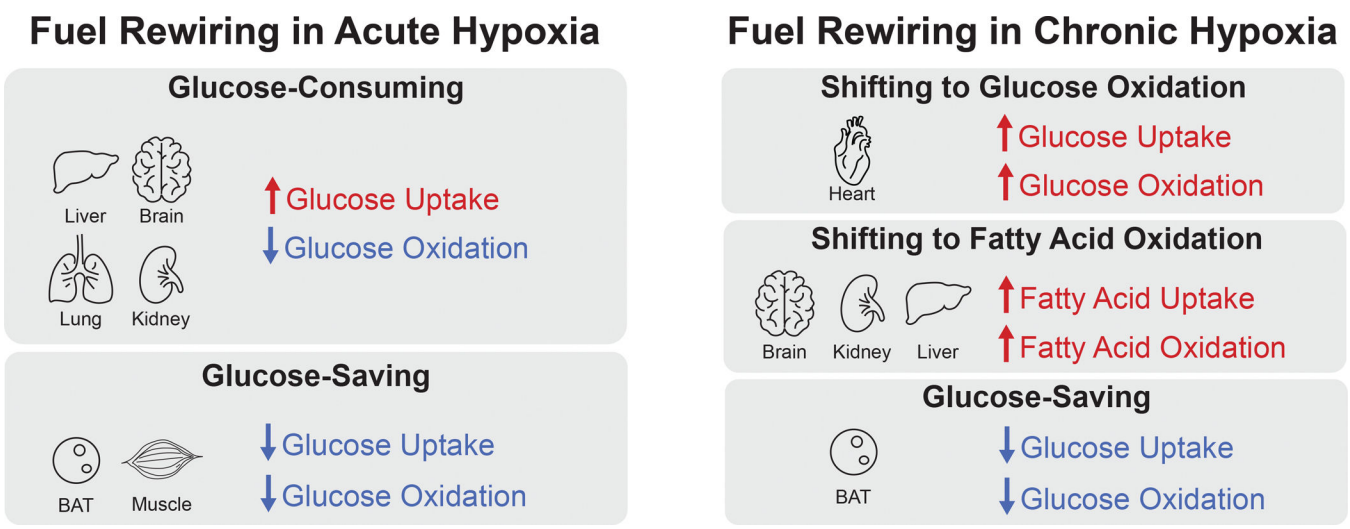

Figure 6. Summary of organ-specific fuel rewiring in physiological adaptation to hypoxia.

Classification of organs that exhibit significant alterations in uptake and mitochondrial oxidation of the circulating fuel sources glucose and palmitate in acute and chronic hypoxia.

Key resources table

REAGENT or RESOURCE	SOURCE	IDENTIFIER
Chemicals, peptides, and recombinant proteins		
U-^{13}C-glucose	Cambridge Isotope Laboratories	Cat#CLM-1396
U-^{13}C-palmitate	Sigma Aldrich	Cat#605573
1,12 Dibromododecane	Sigma Aldrich	Cat#174866-5G
Methyl 3-mercaptoproprionate	Sigma Aldrich	Cat#108987-5G
Oxygen-18 water	Rotem Industries, Ltd	Cat#18-98-050A
FDG Citrate Cassette	GE	Cat#1176837
Fluorine-18 fluoride ion	UCSF Cyclotron	N/A
Critical commercial assays		
i-STAT CHEM8+ Cartridge	Zoetis	Cat#10023291
Zero-oxygen calibration kit	Unisense	Cat#CALKIT-O2
Mouse/Rat Insulin Kit	Meso Scale Discovery	Cat#K152BZC
Mouse Leptin Kit	Meso Scale Discovery	Cat#K152BYC
Glucagon RIA	Millipore Sigma	Cat# GL-32K
Corticosterone Double Antibody RIA Kit	MP Biomedicals	Cat# 0712010-CF
Rat/Mouse Ghrelin (active) ELISA	Millipore Sigma	Cat#EZRGRA-90K
QuantiTect Reverse Transcription Kit	Qiagen	Cat#205311
Maxima SYBR Green/ROX qPCR Master Mix (2X)	Thermo Fisher	Cat#K0222
Experimental models: Organisms/strains		
C57BL/6J	Jackson Laboratory	Strain #: 000664; RRID: MGI:2159769
Oligonucleotides		
Primer sequences for qPCR, see supplemental table 1	This paper	N/A
Software and algorithms		
TraceFinder 5.1 General Quan	Thermo Fisher	N/A
GraphPad Prism	GraphPad	RRID:SCR_002798
ggplot2	Wickham[76]	RRID:SCR_014601
ggsignif	Ahlmann-Eltze and Patil[77]	N/A
AccuCor	Su et al.[75]	N/A
AMIDE	Loening and Gambhir[73]	RRID:SCR_005940